



**HAL**  
open science

# Collisional line broadening and mixing in the Raman spectrum of CO perturbed by N<sub>2</sub>: Experimental measurements and theoretical calculations

D. Paredes-Roibás, R.Z. Martínez, H. Józwiak, Franck Thibault

► **To cite this version:**

D. Paredes-Roibás, R.Z. Martínez, H. Józwiak, Franck Thibault. Collisional line broadening and mixing in the Raman spectrum of CO perturbed by N<sub>2</sub>: Experimental measurements and theoretical calculations. *Journal of Quantitative Spectroscopy and Radiative Transfer*, 2021, 275, pp.107868. 10.1016/j.jqsrt.2021.107868 . hal-03334306

**HAL Id: hal-03334306**





**<https://hal.science/hal-03334306>**

Submitted on 15 Sep 2021

**HAL** is a multi-disciplinary open access archive for the deposit and dissemination of scientific research documents, whether they are published or not. The documents may come from teaching and research institutions in France or abroad, or from public or private research centers.

L'archive ouverte pluridisciplinaire **HAL**, est destinée au dépôt et à la diffusion de documents scientifiques de niveau recherche, publiés ou non, émanant des établissements d'enseignement et de recherche français ou étrangers, des laboratoires publics ou privés.

# Collisional line broadening and mixing in the Raman spectrum of CO perturbed by N<sub>2</sub>: experimental measurements and theoretical calculations

Denís Paredes-Roibás <sup>a,b</sup>, Raúl Z. Martínez <sup>a</sup>, Hubert Jóźwiak <sup>c</sup>,  
Franck Thibault <sup>d</sup>

<sup>a</sup>*Instituto de Estructura de la Materia, IEM-CSIC. Serrano 123, 28006 Madrid, Spain.*

<sup>b</sup>*Departamento de Ciencias y Técnicas Fisicoquímicas, Facultad de Ciencias, Universidad Nacional de Educación a Distancia (UNED), Paseo de la Senda del Rey 9, E-28040 Madrid, Spain.*

<sup>c</sup>*Institute of Physics, Faculty of Physics, Astronomy and Informatics, Nicolaus Copernicus University, Grudziadzka 5, 87-100 Toruń, Poland*


<sup>d</sup>*Univ Rennes, CNRS, IPR (Institut de Physique de Rennes)-UMR 6251, F-35000 Rennes, France*

---

## Abstract

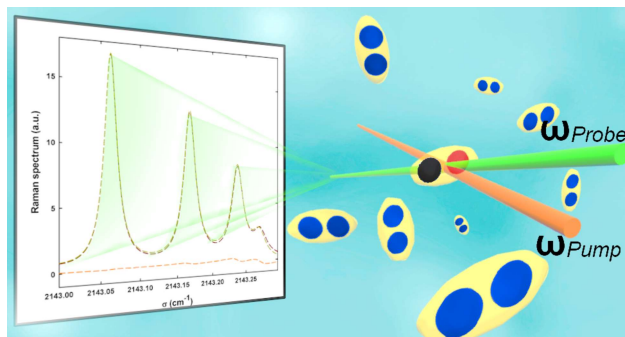
We present a joint experimental and theoretical study of line broadening and mixing in the Q branch of the Raman spectrum of CO perturbed by N<sub>2</sub> at 77, 195 and 298 K. Advanced methods and facilities have been used for both aspects of the study: the experiments were conducted using a high-resolution stimulated Raman spectroscopy setup, while the calculations were performed using a quantum dynamical formalism and one of the most recent potential energy surfaces available. Line broadening coefficients were determined experimentally for rovibrational lines up to  $j = 11$  at 77 K,  $j = 15$  at 195 K and  $j = 19$  at 298 K, and calculated for lines up to  $j = 6$  at the three temperatures. Line mixing was also observed and coefficients measured for lines up to  $j = 8$  at 77 K and  $j = 5$  at 195 K, and again calculated up to  $j = 6$  at the three temperatures. A comparison shows an overall very good agreement between experiments and calculations for both sets of coefficients. Additional calculated data for the pure rotational R and S lines **are** also provided.

---

*Email address:* [denis.paredes@iem.cfmac.csic.es](mailto:denis.paredes@iem.cfmac.csic.es) (Denís Paredes-Roibás )

*Preprint submitted to Journal of Quantitative Spectroscopy and Radiative Transfer August 2, 2021*

## Graphical Abstract



*Keywords:*

Collisional Broadening, Line Mixing, Stimulated Raman Spectroscopy, Quantum Dynamical Calculations, CO-N<sub>2</sub>

### 1. Introduction

2 The CO-N<sub>2</sub> collisional system has been the object of numerous studies in  
3 the last decades. One of the attractions of the system lies in the possible for-  
4 mation of the CO-N<sub>2</sub> dimer and the study of its rovibrational energy levels,  
5 a topic that has seen a renewed interest in the last 10 years [1–4]. However,  
6 most of the attention this collisional system has received stems from its pres-  
7 ence in a number of different environments and from the information that  
8 studies of its spectral features can provide about them. The closest of these  
9 environments is the Earth’s atmosphere, mainly constituted by N<sub>2</sub> but with  
10 a trace presence of CO. The role of CO in different atmospheric processes like  
11 the CO-OH-CH<sub>4</sub> cycle [5, 6], one of the self-cleansing processes of the tro-  
12 posphere, coupled with the fact that part of this atmospheric CO originates  
13 from anthropogenic emissions [5], has attracted considerable interest.

14 Besides Earth, the presence of CO has been reported also in some bodies  
15 of our solar system with weak atmospheres that are covered by different  
16 ices. The sublimation of these ices produces atmospheres in which both CO  
17 and N<sub>2</sub> are present. This is the case of Pluto [7], Titan [8] and Triton [9],  
18 in which significant amounts of both molecules have been found by infrared  
19 spectroscopy. Furthermore, in exoplanetary atmospheres such as those of HD  
20 209458b [10], HD 189733b [11] and WASP-12b [12], among other exoplanets  
21 [13], CO has also been detected. The possibility that CO plays a role in the

22 formation of planetary hazes in these types of atmosphere has been explored  
23 [14].

24 Given that most of the measurements used for the remote determina-  
25 tion of concentrations of molecular species, be it in the Earth's atmosphere,  
26 an exoplanetary atmosphere or an interstellar cloud, are obtained by spec-  
27 troscopic means, both ground- and satellite-based, and that the shape of  
28 molecular spectra strongly depends on temperature and pressure changes, it  
29 is critical to have accurate knowledge of the pressure broadening and shift co-  
30 efficients of the species under study at different temperatures for a successful  
31 extraction of the information contained in these spectra.

32 Other than atmospheric and astrophysical studies, there is also a number  
33 of technological applications in which the CO-N<sub>2</sub> system is involved. The  
34 most important one is probably combustion studies: the technique of coher-  
35 ent anti-Stokes Raman spectroscopy (CARS) is widely used for temperature  
36 measurement in combustion environments, usually through monitorization  
37 of the CARS spectrum of N<sub>2</sub> [15, 16], but also for the determination of the  
38 concentration of species like CO [16], which often appear as minor combus-  
39 tion products. CARS has been used to determine temperatures and products  
40 concentration through monitorization of CO and N<sub>2</sub> spectra in combustion  
41 engines [17], diagnosis of solid propellants [18] or jet diffusions flames [19]  
42 among other combustion applications. Again, a good knowledge of the spec-  
43 tra of these molecules at different temperatures and pressures is key for the  
44 interpretation of the experimental data.

45 Due to the weak dipole moment of the CO molecule, the CO-N<sub>2</sub> collisional  
46 system can be studied using infrared (IR) spectroscopy. This is reflected in  
47 the large number of studies, both experimental and theoretical, performed  
48 on the P and R branches of the fundamental vibration of CO perturbed by  
49 N<sub>2</sub> carried out in the last decades. In particular, Nakazawa et al. [20, 21]  
50 studied the R branch of CO self-perturbed and perturbed by N<sub>2</sub> at several  
51 temperatures. Drascher et al. [22] measured the collisional broadenings and  
52 shifts of R-branch lines perturbed by Ar, N<sub>2</sub>, O<sub>2</sub> and H<sub>2</sub>. Predoi-Cross et al.  
53 [23] studied the broadening and shifting of lines in the P and R branches  
54 of the rovibrational spectrum of CO perturbed by N<sub>2</sub> at 348 K. Besides  
55 the fundamental vibrational band, broadenings, shifts and asymmetries have  
56 also been measured in other IR-active bands like the  $v=0 \rightarrow 2$  [24] and  
57  $v=0 \rightarrow 3$  [25] overtones. There are also a number of other works on specific  
58 pure rotational transitions such as  $j=0 \rightarrow 1$  [26–29],  $j=1 \rightarrow 2$  [29, 30],  
59  $j=2 \rightarrow 3$  [29, 31],  $j=3 \rightarrow 4$  [29], and  $j=4 \rightarrow 5$  [32, 33].



60 The only *ab initio* determination of CO linewidth parameters up to today  
61 was performed recently by Józwiak et al. [34] for the pure rotational R(0)  
62 line. The dynamical calculations to this end were performed on three recent  
63 potential energy surfaces (PES) for the CO-N<sub>2</sub> interacting pair [2–4]. We refer  
64 the reader to the numerous studies devoted to the R lines of CO perturbed  
65 by N<sub>2</sub> listed in Ref. [34].

66 Compared to the number of IR studies, experimental studies of CO per-  
67 turbed by N<sub>2</sub> by means of Raman spectroscopy are scarce in the bibliography,  
68 and nearly all of them focus on pure rotational transitions. Afzelius et al. [35]  
69 obtained rotational CARS spectra in CO-N<sub>2</sub> mixtures in order to compare  
70 the experimental linewidths with the ones predicted by their model. More  
71 recently, collisional line broadening measurements on the pure rotational S  
72 branch of the Raman spectrum of CO perturbed by N<sub>2</sub> were performed by  
73 Hsu et al. [36]. An experimental study closer to the one presented in this  
74 article was conducted years ago by Roblin et al. [37]. CARS was used to  
75 record the Q branch of the fundamental vibration of CO perturbed by N<sub>2</sub>.  
76 The experiment, however, was performed at pressures between 1 and 100  
77 atm, a much higher regime than the one explored in the present work, and  
78 the authors did not attempt to obtain experimental broadening or mixing  
79 coefficients.

80 Theoretical studies of line broadening and mixing coefficients for rovibra-  
81 tional Raman lines in this collisional system are also scarce. In the work  
82 of Roblin *et al.* [37], the transfer of intensity between lines due to line  
83 mixing was modeled via the semi-empirical modified energy gap law, the  
84 parameters of which were adjusted on the linewidths derived from the semi-  
85 classical method of Robert-Bonamy. The most recent calculation of Raman  
86 line broadening coefficients to date was performed by Afzelius et al. [38].  
87 Using the Robert-Bonamy formalism, the authors calculated line broaden-  
88 ing coefficients for the isotropic Raman Q branch lines of the fundamental  
89 vibration of CO perturbed by N<sub>2</sub>, as well as for infrared R lines.

90 This work presents a study, both experimental and theoretical, of line  
91 broadening and mixing in the Raman spectrum of the fundamental vibra-  
92 tional band of CO perturbed by N<sub>2</sub> at 77, 195 and 298 K. Collisional line  
93 broadening and line mixing coefficients for the rovibrational lines in the Q  
94 branch of the band have been obtained by means of high resolution Raman  
95 spectroscopy and quantum dynamical calculations at three different temper-  
96 atures. Both approaches are described in detail in the following sections.

## 97 2. Experimental part

### 98 2.1. Methods

99 The spectral line profiles analyzed in this work belong to rovibrational  
100 lines of the Q branch ( $\Delta j = 0$ ) in the Raman spectrum of the fundamental vi-  
101 bration ( $v=0 \rightarrow v=1$ ) of the molecule of CO perturbed by collisions with N<sub>2</sub>.  
102 The high resolution Raman spectra required for these analyses were obtained  
103 by means of an experimental setup based on the technique of stimulated Ra-  
104 man spectroscopy (SRS). SRS was initially demonstrated by Owyong with  
105 continuous (cw) laser sources [39], but the relatively low sensitivity of the  
106 technique led to the development of the quasi-continuous (quasi-cw) scheme  
107 in which one cw and one pulsed laser source are used [40, 41]. Our setup  
108 follows this quasi-cw scheme. Through the years, different variations of the  
109 experimental setup have been used in our laboratory to obtain high resolution  
110 Raman spectra of rovibrational and pure rotational transitions for frequency  
111 [42], line profile [43] and even collisional energy transfer [44] studies. For the  
112 present work we set up a configuration similar to the one described in [45],  
113 with a number of relevant differences and modifications that are described  
114 in detail in the following paragraphs. An updated schematic layout of our  
115 setup is depicted in Fig. 1.

116 The cw probe beam is generated by a single-mode Ar<sup>+</sup> ion laser (Spectra-  
117 Physics 2080) tuned to the 529 nm emission line. The laser is frequency-  
118 stabilized and actively locked to a molecular reference, a hyperfine component  
119 of the electronic absorption spectrum of <sup>130</sup>Te<sub>2</sub> in the vapor phase. The tran-  
120 sition at 18909.44611 cm<sup>-1</sup>, measured in our laboratory [46], has been used  
121 as reference throughout this work. The system is able to reach a linewidth,  
122 determined by the residual jitter, lower than 500 kHz ( $1.7 \times 10^{-5}$  cm<sup>-1</sup>). The  
123 output power of the laser is set to  $\sim 500$  mW.

124 The pump beam is obtained by pulsed optical amplification of a cw tun-  
125 able seed generated by a single-mode cw ring dye laser (Sirah Mattisse DS),  
126 operated with a solution of Rhodamine 6G for this experiment. A three-stage  
127 pulsed dye amplifier (Quanta-Ray PDA-1) with a solution of Kiton Red and  
128 pumped by the second harmonic of a 10 Hz Nd:YAG laser is used for the  
129 optical amplification of the cw seed. The resulting tunable pulses have near-  
130 Gaussian temporal and spectral shapes with  $\sim 12$  ns of temporal full width  
131 at half maximum (FWHM) and  $\sim 70$  MHz of spectral FWHM. Pulse energies  
132 of several tens of mJ can be reached.

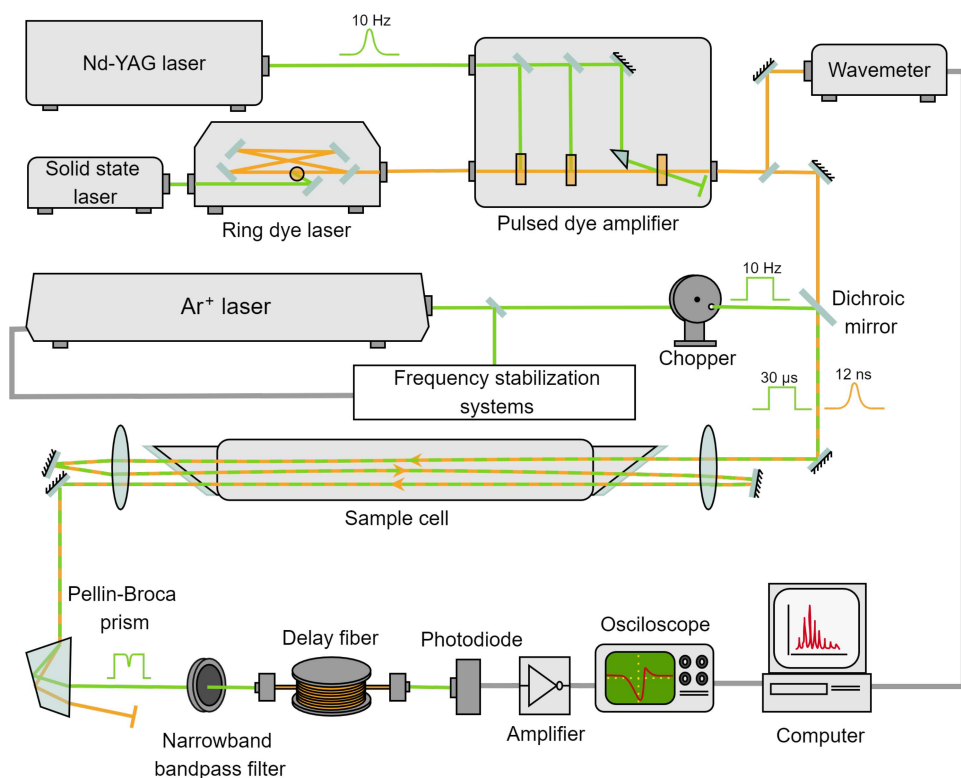


Figure 1: Schematic experimental setup of the stimulated Raman loss experiment. For the sake of simplicity some of the elements mentioned in the text have been omitted.

133 Raman frequencies are obtained at any point by simple subtraction of  
 134 the frequencies of the probe and pump beams. The frequency of the locked  
 135 probe beam is well known and kept constant throughout the experiment,  
 136 while the frequency of the tunable pump beam needs to be measured at  
 137 every point (pulse). This task is performed by a high accuracy wavemeter  
 138 (HighFinesse WSU-10), which provides a nominal accuracy of 10 MHz ( $3\sigma$ )  
 139 and is periodically calibrated using as a reference radiation a fraction of the  
 140 frequency-locked probe beam.

141 Two different sample cells were used for this work, one made of Pyrex  
 142 glass and the other one of stainless steel, in order to reach the various sample  
 143 temperatures at which spectra were recorded. The Pyrex cell, consisting of  
 144 a central cylindrical sample chamber and surrounding coolant and isolation  
 145 chambers, has already been described in prior works [45, 47]. In the present

146 one it was used for the obtention of the 77 K spectra, with liquid nitrogen  
147 as coolant, and of the 298 K spectra. The stainless steel cell follows a simi-  
148 lar design philosophy: an inner sample chamber of cylindrical shape with a  
149 length of  $\sim 90$  cm, an internal diameter of 2.5 cm and ultraviolet fused silica  
150 (UVFS) windows installed on both ends at Brewster's angle. The central  
151 part of this cylinder, up to a few centimeters from each end, is enclosed by a  
152 second, cuboidal-shaped stainless steel structure with its top face open (i.e. a  
153 stainless steel "box"). This box acts as a container for the coolant and allows  
154 the central body of the cell to be submerged in it. The outside of the box is  
155 insulated with a layer of styrofoam. This cell was used for the obtention of  
156 the 195 K spectra with dry ice as coolant.

157 Prior to its arrival to the sample cell, the probe beam goes through an elec-  
158 tromechanical modulator ("chopper") synchronized with the Nd:YAG laser  
159 clock to produce square "pulses" of  $30 \mu\text{s}$  width at a repetition rate of 10  
160 Hz to avoid saturation of the detection photodiode. The probe and pump  
161 beams, both vertically polarized, are spatially overlapped by means of a  
162 dichroic mirror, focused into the sample cell by an  $f=500$  mm lens and rec-  
163 ollimated by a similar lens after the cell. A triple pass is used to increase  
164 the sensitivity of the experiment. After this, the two beams are separated  
165 using two Pellin-Broca prisms. The pump beam is dumped, while the probe  
166 beam passes through a narrowband bandpass filter (Semrock MaxLine LL01-  
167 532-12.5) to block any residual pump light and is injected into a 100 m long  
168 multimode fiber. The role of the fiber is to introduce a delay of  $\sim 400$  ns  
169 in the detection of the Raman signal being carried by the probe beam, so  
170 that this detection and measurement stage is not affected by the electrical  
171 noise associated to the Q-switch electronics of the Nd:YAG laser. At the  
172 output of the fiber, the probe radiation is refocused on the surface of a fast  
173 PIN photodiode (EG&G FND-100). The electrical output of this photodiode  
174 passes through a high-pass filter that removes the DC components and is fed  
175 to a transimpedance amplifier (FEMTO HCA-400M-5K-C), whose output is  
176 sent to a digital oscilloscope (Tektronix DPO7254) operating in Fast Frame  
177 (hardware-driven) mode. The oscilloscope, triggered synchronously by the  
178 Nd:YAG laser clock, digitizes and stores all the traces. Each one of these  
179 traces contains information about variations in the intensity of the probe  
180 laser in the temporal window corresponding to its interaction with a pump  
181 laser pulse inside the sample cell. Analyses of these data are performed in a  
182 separate computer with code specifically developed by us using the Matlab  
183 package, which carries out the necessary numerical integration of the traces

184 as well as additional noise filtering, frequency assignment to each data point  
185 and other postprocessing tasks to produce the final Raman spectrum.

186 CO and N<sub>2</sub> were provided by Air Liquide with purities >99.997% and  
187 >99.999% respectively. Prior to the obtention of CO-N<sub>2</sub> Raman spectra,  
188 several preparation runs were conducted with samples of pure CO at low  
189 pressures (2 to 8 mbar) and at the three temperatures of interest. These  
190 runs accomplished two main objectives:

- 191 • The determination of the Gaussian contribution present in the line pro-  
192 files at each one of these temperatures. To this end, the experimental  
193 lines were fitted with Voigt profiles, and the results confirmed a minimal  
194 Lorentzian contribution, as expected at these pressures, and a domi-  
195 nant Gaussian contribution. This Gaussian contribution results from  
196 the convolution of the Doppler profile and the apparatus function, both  
197 of which are also Gaussian. Since the Doppler contribution for any line  
198 at a given temperature can be easily calculated, these measurements  
199 also allowed us to extract a value for the width of our Gaussian appa-  
200 ratus function, which was quantified as  $0.0021 \pm 0.0001 \text{ cm}^{-1}$  FWHM.
- 201 • The determination of the optimum energy level for the pump pulses.  
202 While higher energies produce larger Raman signals, the spectral pro-  
203 files also start to experience broadening and develop an asymmetry due  
204 to the AC Stark effect induced by the intense electromagnetic field of  
205 the laser pulses. Using a variable attenuator, trials were conducted at  
206 several pump pulse energies, and 10 mJ was determined to be the high-  
207 est pulse energy past which —under our focusing conditions— Stark  
208 broadening started to be detectable in the line profiles. Consequently,  
209 all the spectra recorded for this work have been obtained with an energy  
210 of 10 mJ/pulse in the pump beam.

211 A CO partial pressure of 5% was used in all the CO-N<sub>2</sub> gas mixtures at  
212 all temperatures. The mixtures were prepared *in situ* in the same sample  
213 cell used to register the spectra and pressures were monitored at all times  
214 by means of capacitive gauges. After performing several tests, the following  
215 nominal pressure values were selected at each temperature:

- 216 • At 298 K, spectra were recorded at 20, 50, 80, 120 and 160 mbar of  
217 total pressure.
- 218 • At 195 K, spectra were recorded at 10, 25, 50, 80 and 110 mbar.

219 • At 77 K, spectra were recorded at 5, 12.5, 20, 30, 40 and 60 mbar.

220 Every spectrum was recorded at least twice at each nominal pressure. The  
221 scan speeds were adjusted according to the width of the spectral lines being  
222 registered, typically between 30 and 60 MHz/s. This translated into the  
223 experimental line profiles being sampled with between 40 and 60 points per  
224 FWHM.

## 225 2.2. *Experimental results*

226 Figure 2 presents three Q-branch spectra of CO perturbed by N<sub>2</sub> recorded  
227 in the course of this work, each one of them registered at one of the three  
228 selected temperatures. The nominal pressures of the spectra in the figure  
229 have been chosen so that the number densities of CO in the sample cell  
230 were similar for the three spectra, and they have been normalized to have  
231 the same maximum height. A simple visual inspection of the baseline noise  
232 reveals how, as temperature is reduced, the signal-to-noise (S/N) ratio of the  
233 spectrum improves due to the total population of the  $v=0$  vibrational level  
234 being distributed among fewer rotational states. An additional contributing  
235 factor is that the peaks in the three spectra being compared get slightly  
236 narrower due to the diminishing Doppler width.

237 For the 298 K spectra, rovibrational lines from Q(0) to Q(19) of the  
238 band could be registered with a good enough S/N ratio to provide reliable  
239 broadening data at all the pressures detailed at the end of Sec. 2.1. This  
240 interval is reduced to Q(0)-Q(15) at 195 K and Q(0)-Q(11) at 77 K. Despite  
241 the relatively low pressures used, the close proximity between rovibrational  
242 components in the band is enough to also produce detectable line interference,  
243 especially in the band head. We were able to obtain line mixing coefficients  
244 for all lines between Q(0) and Q(8) at 77 K and between Q(0) and Q(5) at  
245 195 K. At 298 K, the poorer S/N ratio of the spectra prevented a similar  
246 determination, so we are unable to provide line mixing coefficients at this  
247 temperature.

248 The initial analysis of the line profiles in the spectra was carried out by  
249 performing multi-peak fits of the whole Q-branch spectrum. This procedure  
250 was conducted independently for each spectrum obtained at a given temper-  
251 ature and pressure. For the selection of the profiles used in the fits, and given  
252 that our spectra were obtained in a relatively low pressure range and that the  
253 two colliding molecules have the same mass, we initially considered a soft-  
254 collision (Galatry) profile. However, after testing the profile with different

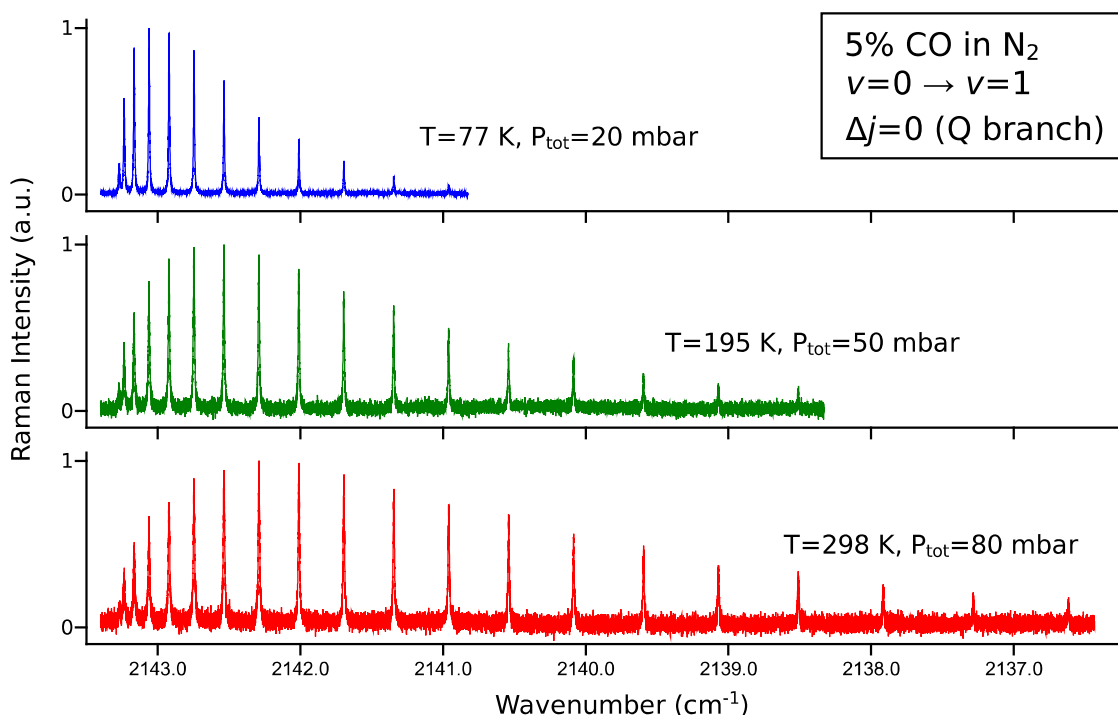


Figure 2: Q-branch spectra of the fundamental band of CO perturbed by N<sub>2</sub> at 77, 195 and 298 K. The nominal pressures have been selected to provide similar number densities.

255 isolated lines in the spectra at different pressures, it became clear that no  
 256 significant deviation from a Voigt profile (i.e., no Dicke narrowing) could be  
 257 detected, at least under our experimental conditions and S/N ratio. Thus,  
 258 Voigt profiles were selected for the fits. Notice that this initial analysis does  
 259 not take into account the possible existence of line mixing.

260 The Voigt fits were initially conducted with both the Gaussian and Lorentzian  
 261 widths left unconstrained for each line. After verifying that the Gaussian  
 262 widths obtained across the whole band matched the one previously deter-  
 263 mined from the spectrum of pure CO at that temperature within the error  
 264 of the fit for most of the lines, these Gaussian widths were constrained to  
 265 that value for all lines and the Voigt fits were repeated, this time with only  
 266 the Lorentzian width unconstrained. This procedure allows a more accurate  
 267 determination of the Lorentzian widths of the weakest lines in the band, as  
 268 well as being particularly useful when there is a large difference between the

269 Gaussian and Lorentzian contributions to the line profile. Figure 3 presents  
 270 an example of one of the Voigt fits of an isolated rovibrational line at 195 K.  
 271 No special pattern can be observed in the residuals.

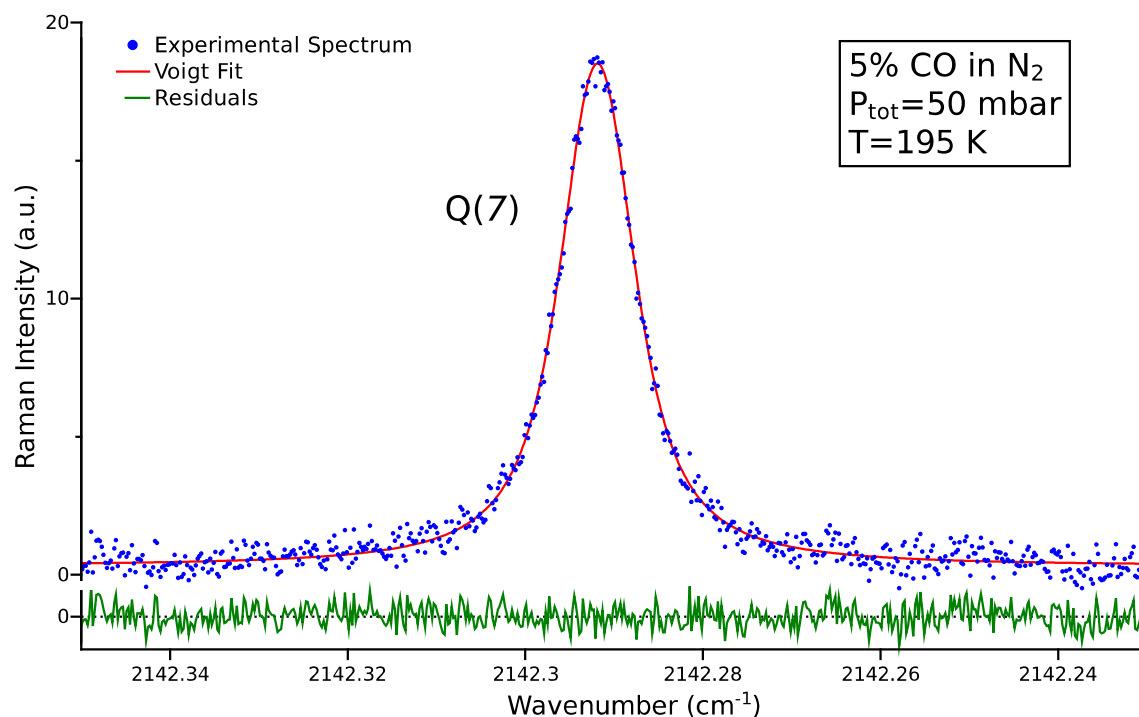


Figure 3: Example of a Voigt fit of the Q(7) rovibrational line at 195 K and a total pressure of 50 mbar. The Gaussian and Lorentzian widths are 0.00450 and 0.00795  $\text{cm}^{-1}$  respectively. Residuals are plotted in the same vertical scale as the experimental spectrum.

272 Following this fitting procedure, a set of Lorentzian widths at different  
 273 pressures is extracted for each rovibrational component of the band at each  
 274 temperature. These widths are then subjected to a simple linear fit, the slope  
 275 of which renders the collisional broadening coefficient for each line. Figure 4  
 276 presents an example of the fits corresponding to the Q(4) line at the three  
 277 temperatures of reference. It is clearly visible how the error bars assigned to  
 278 the experimentally determined half widths at half maximum (HWHM) are  
 279 larger for the higher temperatures. Despite this, and except for the first lines  
 280 of the band—for which line mixing is noticeable as discussed below—the  
 281 variation of the collisional widths with pressure is remarkably well fitted by  
 282 this linear model in the range of pressures under study.



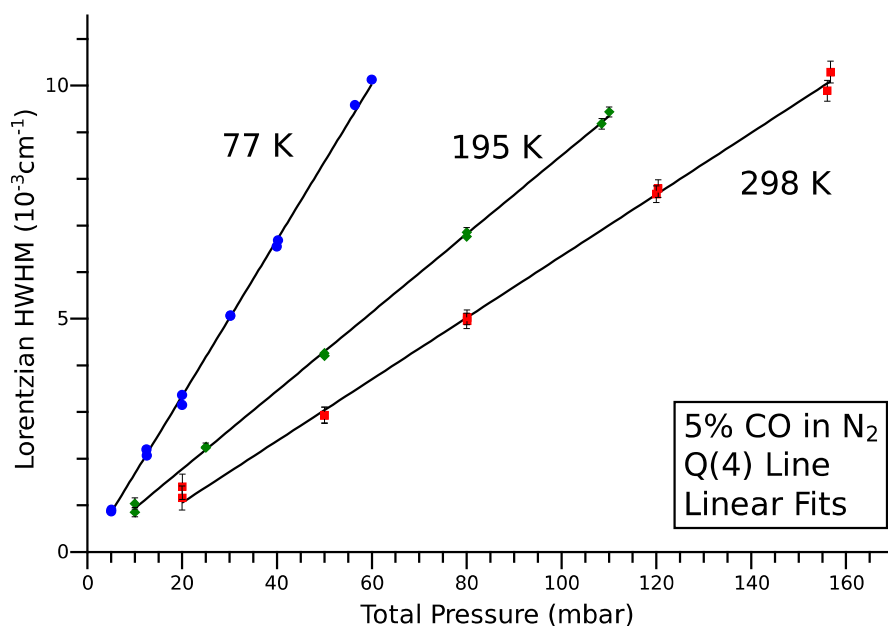


Figure 4: Variation of the Lorentzian HWHM with pressure for the Q(4) line at the three experimental temperatures. The black lines represent linear fits of the data at each temperature. Error bars represent 1 standard error. Due to the small magnitude of the error intervals they are contained within the symbols at 77 K.

283 For the very first lines of the band, however, the residuals indicate that  
 284 the use of Voigt profiles is not totally satisfactory. The effect, although subtle  
 285 in our spectra at the relatively low pressures at which we have worked, indi-  
 286 cates the presence of line mixing and is especially visible at 77 K due to the  
 287 more favorable S/N ratio. Line mixing can be thought of as the consequence  
 288 of an interference between the different paths that a molecule in a certain  
 289 initial state can take to reach a final excited state ( $v=0, j=j \rightarrow v=1,$   
 290  $j=j$  in our Q-branch example) when it is optically excited in the presence  
 291 of significant collisional relaxation. Molecular collisions open new potential  
 292 transition paths in which—for example—a molecule in  $v=0, j=j$  could  
 293 first be collisionally promoted to  $v=0, j=j+1$ , then undergo radiative  
 294 excitation (in our case via a Raman process) to  $v=1, j=j+1$ , and finally  
 295 relax, again through collisions, to  $v=1, j=j$ . This is an alternative path  
 296 to the direct optical one with the same departure and destination states and  
 297 with the optical part of the excitation having taken place through a differ-

298 ent Q-branch transition. The presence of these alternative paths creates an  
 299 interference that appears as cross-terms in the calculation of the transition  
 300 probabilities [48, 49]. In density matrix formalism, this phenomenon is char-  
 301 acterized as a flow between different components of the optical coherence,  
 302 i.e., the off-diagonal terms of the density matrix which couple different states  
 303 of the active molecule, mediated by collisions [50, 51].

304 From an observational point of view, line mixing manifests itself as a  
 305 transference of intensity from one region of the spectrum to another, thus  
 306 altering the overall shape of the spectral band, sometimes dramatically if the  
 307 coupling between lines is very strong. In a case like ours, in which the low  
 308 pressures used produce only moderate line overlapping, the coupling is weak  
 309 and an adequate line mixing model, as confirmed by prior works on this very  
 310 band [52, 53], is the profile of Rosenkranz [54]. Following Eq. (17) in Ref. 53  
 311 and Eq. (1) in Ref. 55 the intensity profile of the band at a given pressure  
 312 can be described by the expression

$$I(\omega) = \sum_j S_j \frac{\Gamma_j + Y_j (\omega - \omega_j - \Delta_j)}{(\omega - \omega_j - \Delta_j)^2 + \Gamma_j^2}. \quad (1)$$

313 In this expression  $S_j$  are the line weights,  $\Gamma_j$  and  $\Delta_j$  are the collisional  
 314 linewidths (HWHM) and shifts,  $\omega_j$  are the central frequencies of the un-  
 315 perturbed lines and  $Y_j$  are the line mixing coefficients. The parameters  $\Gamma_j$ ,  
 316  $\Delta_j$  and  $Y_j$  have a linear dependence with pressure in Rosenkranz's first-order  
 317 approximation [54]. The shape of the whole band can thus still be calculated  
 318 as a sum of the independent contributions of each rovibrational component,  
 319 which can in turn be separated into one Lorentzian and one dispersive contri-  
 320 bution. This expression accounts for the purely collisional contribution to the  
 321 experimental linewidths: in order to compare it to the experimental spectra,  
 322 the result of Eq. (1) needs to be convolved with the Gaussian contributions  
 323 (Doppler + apparatus function) present in our spectra. To this end, a min-  
 324 imization Matlab code was developed to calculate a synthetic Rosenkranz  
 325 profile according to Eq. (1), perform the convolution with the known Gaus-  
 326 sian component numerically, and find the values of the parameters in Eq. (1)  
 327 that minimize the difference between the calculated and experimental bands.  
 328 When this code is run on an experimental spectrum, we obtain fitted values  
 329 for the  $Y_j$  line mixing coefficients and  $\Gamma_j$  Lorentzian linewidths of each Q( $j$ )  
 330 rovibrational component of the band at that pressure and temperature. Line  
 331 shifts in this band are expected to be between one and two orders of mag-

332 nitude smaller than line broadenings [56–60], so we ignore them by simply  
333 considering  $(\omega_j - \Delta_j)$  a single parameter in the fit. For a given rotational  
334 component  $Q(j)$  at a given temperature several  $Y_j$  are obtained, one for each  
335 pressure at which the band has been recorded. By simply performing a linear  
336 fit of these  $Y_j$  coefficients against the pressure we obtain as slope a pressure-  
337 independent line mixing coefficient for that rotational line that we denote by  
338  $Y_j^p$ , with  $Y_j^p \cdot p = Y_j$ .

339 The procedure described above was attempted with all the spectra recorded  
340 for this work at all temperatures, but the S/N ratio of the 298 K spectra did  
341 not allow a reliable determination of the line mixing coefficients from the  
342 experimental data. We have been able to obtain values for the coefficients  
343 and their associated collisional linewidths for the rovibrational lines between  
344  $j = 0$  and  $j = 8$  at 77 K and between  $j = 0$  and  $j = 5$  at 195 K. An example  
345 of one of the fits of the experimental spectra, in this case at 77 K, is presented  
346 in Fig. 5, with the Lorentzian and dispersive contributions to the overall fit  
347 displayed separately. As expected, the Raman scattering is sublorentzian in  
348 the high wavenumber side of the band head while it is superlorentzian in the  
349 first microwindows.

350 The deviations of the Lorentzian linewidths  $\Gamma_j$  obtained from convolved  
351 Rosenkranz profiles with respect to the ones obtained with Voigt profiles are  
352 noticeable only for the first rovibrational lines of the band, with  $Q(0)$  being  
353 the most affected one. They become negligible, for our standard error in-  
354 tervals, beyond  $Q(3)$ , where the widths determined by both the Voigt and  
355 Rosenkranz models converge. To illustrate the error introduced by the hy-  
356 pothetical neglect of line mixing in the analysis of these first components,  
357 Fig. 6 presents, for  $Q(0)$  at 77 K, a comparison between the Lorentzian  
358 linewidths extracted from the spectra at different pressures with the Voigt  
359 and Rosenkranz models. When a linear fit is used on both sets of data to  
360 determine the collisional broadening coefficient it is clear that the Voigt data  
361 consistently underestimates the width of the rotational line. Since the ef-  
362 fect grows markedly with pressure, the widths at higher pressures are more  
363 affected and a “blind” linear fit of Voigt data would end up yielding a signif-  
364 icantly lower ( $\sim 20\%$ ) value for the collisional broadening coefficient for this  
365 line.

366 Experimental values for the collisional broadening coefficients of CO per-  
367 turbed by  $N_2$  at 77, 195 and 298 K are plotted on Fig. 7. The coefficients  
368 at 77 and 195 K have been obtained using the Rosenkranz model described  
369 above, which renders the same result as a multi-peak Voigt fit for  $j > 3$ ,

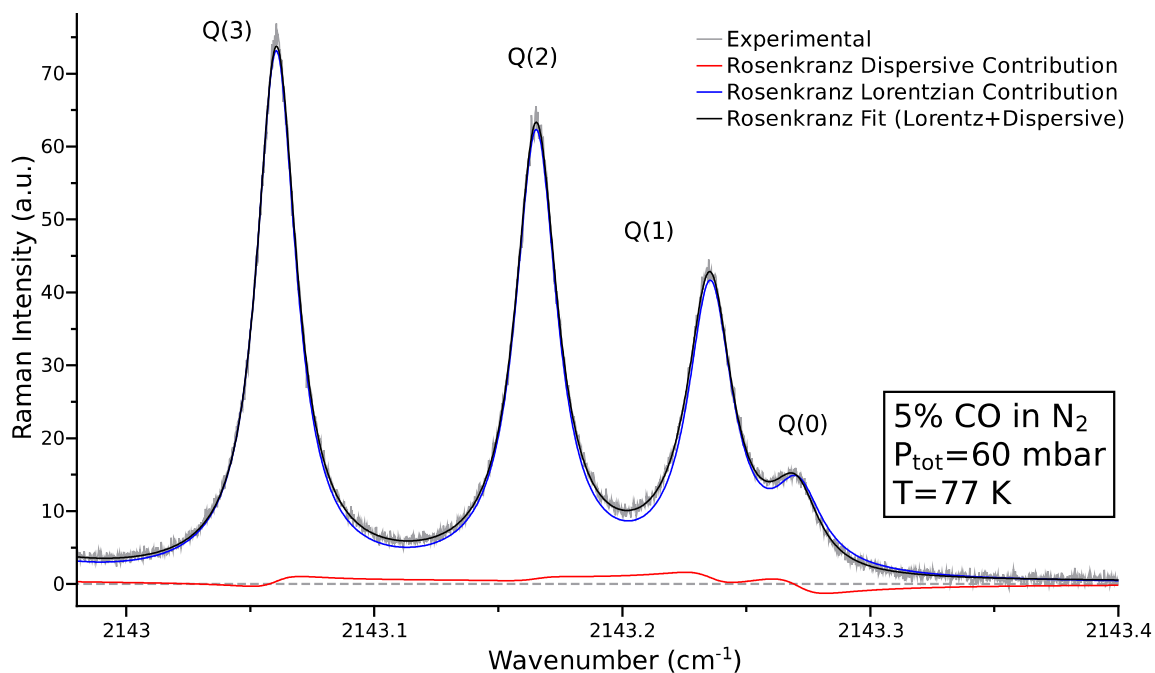


Figure 5: Rosenkranz fit of the first CO Q-branch lines at 77 K and a total pressure of 60 mbar. The Lorentzian and dispersive contributions to the overall Rosenkranz profile are displayed separately to illustrate their relative magnitudes. They have already been convolved with a Gaussian function of  $0.0033 \text{ cm}^{-1}$  FWHM in order to reproduce the experimental data.

370 while the ones at 298 K have been obtained with Voigt profiles.

371 Figure 8 presents the values obtained for the  $Y_j^p$  line mixing coefficients.  
 372 It is clear that the effect of line mixing in the spectrum is more noticeable in  
 373 the first lines but becomes smaller as  $j$  grows and line overlap decreases.

374 The determination of the theoretical values reported in Figs. 7 and 8 is dis-  
 375 cussed in the next section. Before doing so, some experimental aspects merit  
 376 to be further discussed. We considered but rejected the possibility of intro-  
 377 ducing a correction in the coefficients to account for CO self-perturbation:  
 378 according to the bibliographic data available at 298 K, both experimental  
 379 [52] and calculated [38], the line broadening coefficients for the Raman lines  
 380 of pure CO in its Q branch have values that are only between 1 and 10%  
 381 higher, depending on the rotational quantum number, than the coefficients  
 382 we have obtained for the same lines in the CO-N<sub>2</sub> system. That the differ-  
 383 ence is small is not surprising given that both molecules have similar masses

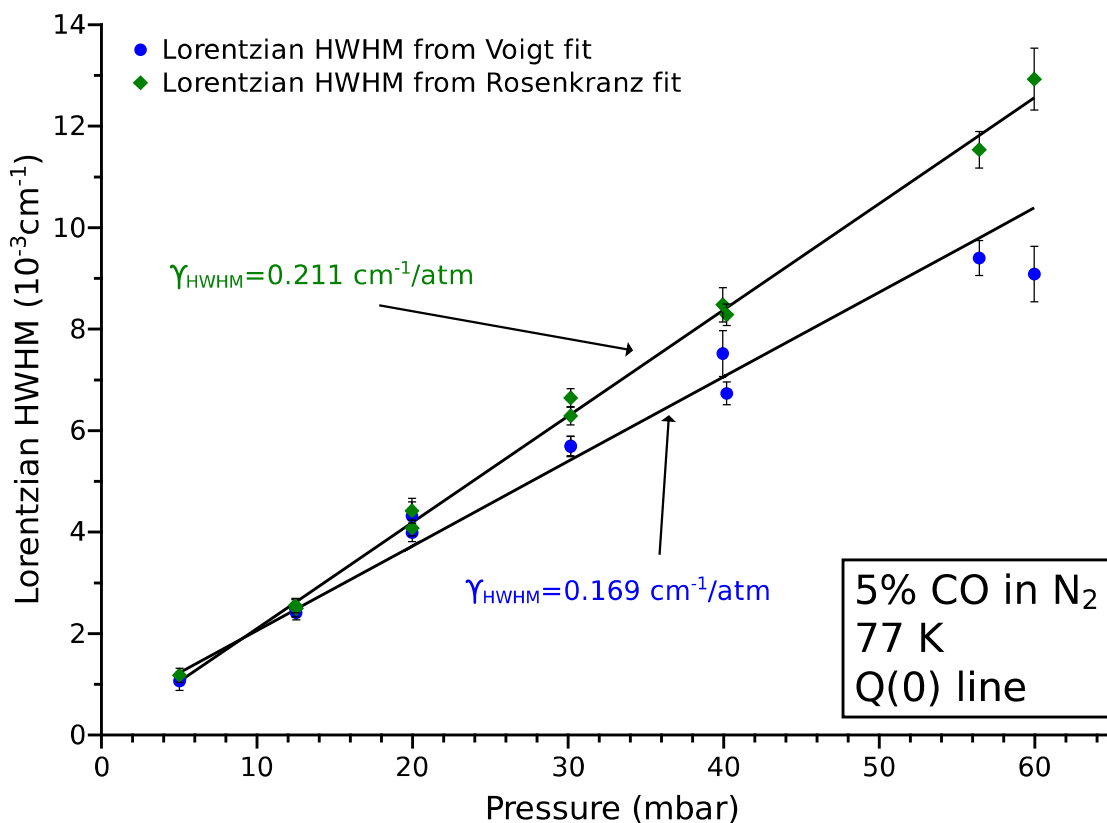


Figure 6: Comparison of linear fits of the collisional HWHMs extracted for Q(0) at 77 K using a Voigt profile (circles) and a Rosenkranz profile (diamonds). Error bars represent 1 standard error.

384 and the dipole moment of CO is rather weak. Since our CO-N<sub>2</sub> mixtures  
 385 contain a 5% of CO, and working under the assumption of a simple addi-  
 386 tive behavior, our experimentally determined coefficients for CO-N<sub>2</sub> would  
 387 be overestimating the “real” coefficients by a maximum of 0.5% in the worst  
 388 case. This is significantly smaller than the uncertainty associated to our  
 389 measurements (see Fig. 7). One final aspect that needs to be addressed in  
 390 order to perform a comparison between our experimental broadening and  
 391 mixing coefficients and calculated ones is the influence of the experimental  
 392 polarization arrangement on the isotropic/anisotropic origin of the intensity  
 393 of the spectral lines. Besides the population and degeneracy of the rovibra-

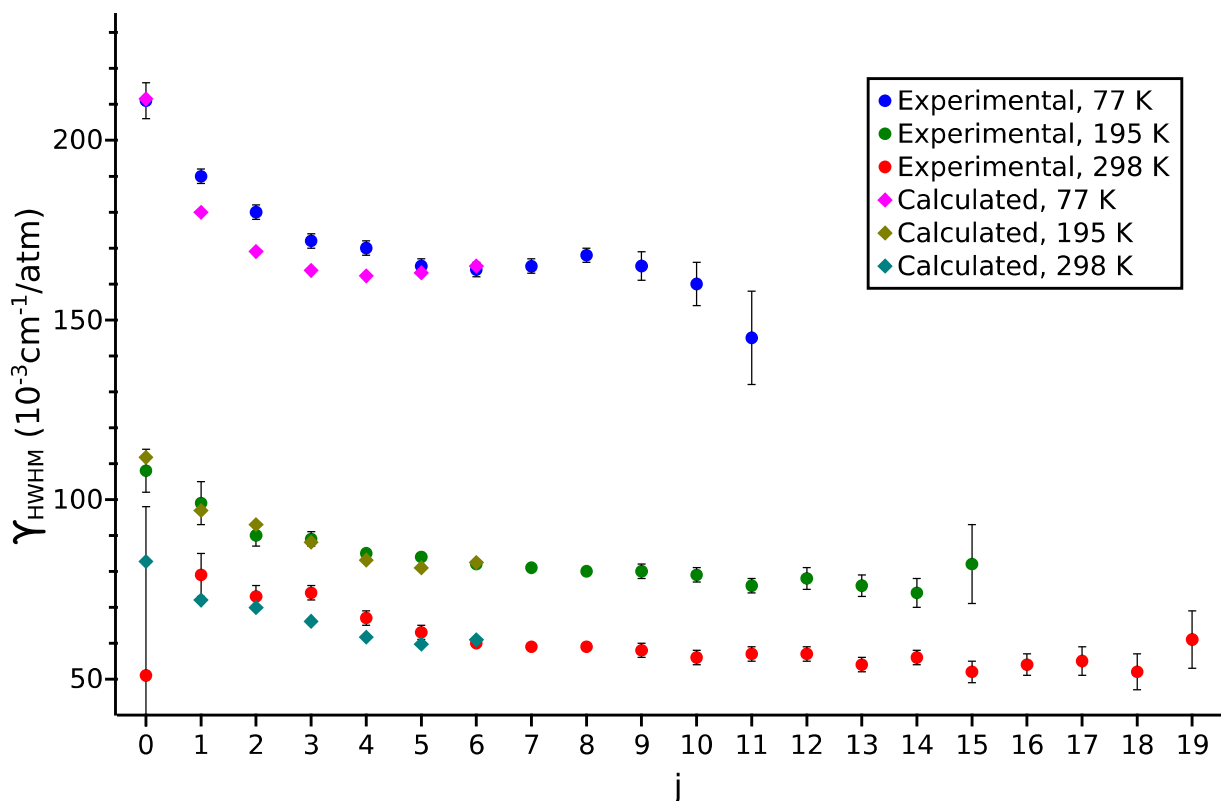


Figure 7: Comparison between experimental and calculated values for the pressure broadening coefficients of CO in N<sub>2</sub> at 77, 195 and 298 K. Error bars in the experimental data represent 1 standard error.

394 tional levels, the observed intensity of a Q-branch Raman transition depends  
 395 on the Placzek-Teller coefficients, the polarizability tensor invariants and the  
 396 polarizations of the excitation and scattered radiations in the experimental  
 397 layout. For an arrangement with parallel polarizations in the two beams, like  
 398 the one we have used in this experiment, the dependence of the intensity  $I_j$   
 399 of a given line Q( $j$ ) on these factors is described by the equation [61]

$$I_j \propto \alpha'^2 + \frac{4}{45} \frac{j(j+1)}{(2j-1)(2j+3)} \gamma'^2, \quad (2)$$

400

401 where  $\alpha'$  and  $\gamma'$  are the derivatives of the trace and anisotropy invariants,  
 402 respectively, of the Raman polarizability tensor. From Eq. (2) it clearly

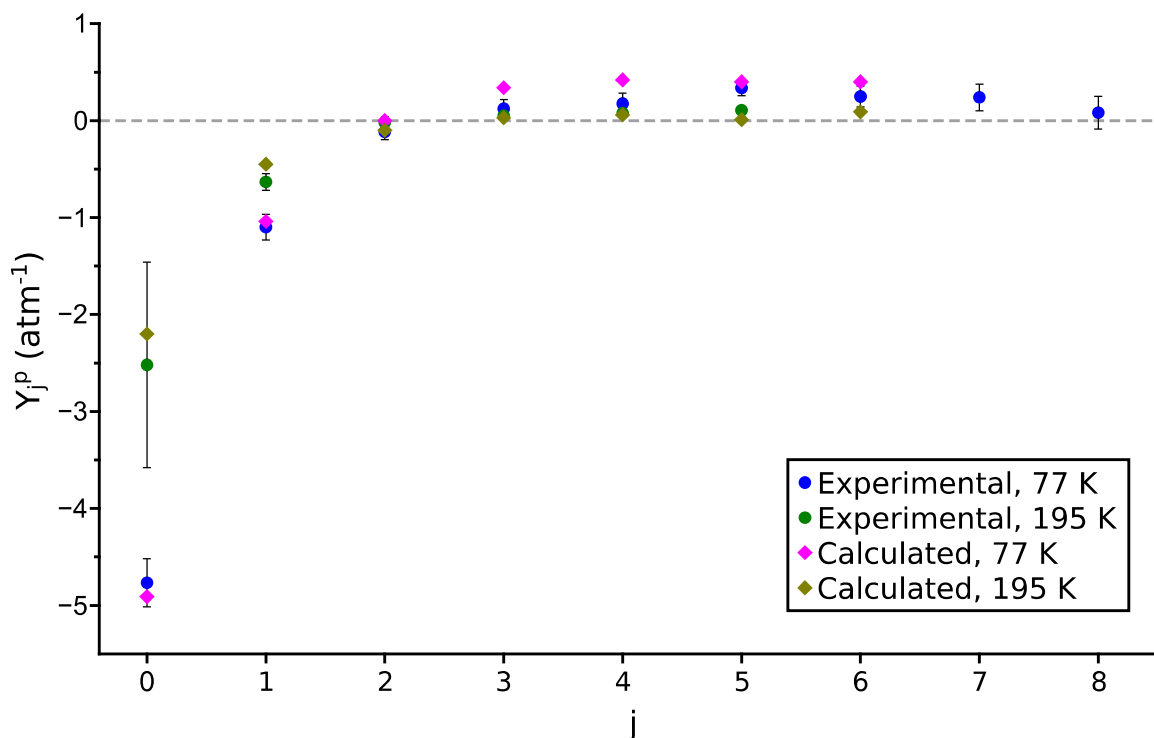


Figure 8: Comparison between experimental and calculated values for the Rosenkranz line mixing coefficients  $Y_j^p$  of CO in  $N_2$  at 77 and 195 K. Error bars in the experimental data represent 1 standard error.

403 follows that the intensity of a Raman Q-branch transition recorded with par-  
 404 allel polarizations has both an isotropic (dependent on  $\alpha'$ ) and an anisotropic  
 405 (dependent on  $\gamma'$ ) contribution, with only the Q(0) line being always purely  
 406 isotropic. In order to calculate these contributions, we rewrite Eq. (2) as

$$I_j \propto 1 + \frac{4}{45} \frac{j(j+1)}{(2j-1)(2j+3)} \left( \frac{\gamma'}{\alpha'} \right)^2. \quad (3)$$

407 The ratio  $\left( \frac{\gamma'}{\alpha'} \right)$  can be obtained from the total band depolarization ratio,  
 408 defined as

$$\rho = \frac{3\gamma'^2}{45\alpha'^2 + 4\gamma'^2} \quad (4)$$

| $j$         | 0    | 1      | 2      | 3      | 4      | 5      | 6      |
|-------------|------|--------|--------|--------|--------|--------|--------|
| $I_{ISO}$   | 100% | 92.68% | 94.66% | 95.00% | 95.12% | 95.18% | 95.22% |
| $I_{ANISO}$ | 0%   | 7.32%  | 5.34%  | 5.00%  | 4.88%  | 4.82%  | 4.78%  |

Table 1: Calculated percentage of isotropic and anisotropic intensity in the Raman Q-branch lines of the CO fundamental recorded with parallel polarizations.

409 and for which several experimental measurements are available. These have  
410 been gathered in a previous work [53], where a value of  $2.22 \pm 0.05$  was  
411 proposed for  $\left(\frac{\gamma'}{\alpha'}\right)^2$ . Based on this number, Tab. 1 presents the calculated  
412 percentage of isotropic and anisotropic contributions to the intensity of the  
413 first components of the Q branch of CO. It can be seen that the anisotropic  
414 contribution is usually very small, of the order of five percent of the total  
415 intensity (it approaches 4.7% asymptotically). This is the reason why  
416 Q-branch Raman spectra of vibrations with low depolarization ratios like  
417 the present one are often approximated as “isotropic spectra”, even though  
418 technically they are not purely isotropic beyond Q(0). The broadening and  
419 mixing coefficients we have obtained experimentally are thus a mixture of  
420 isotropic and anisotropic coefficients, but if to the small relative size of the  
421 anisotropic contribution we add the fact that the isotropic and anisotropic  
422 coefficients are normally very close in value (see for example Ref. 47, where  
423 both sets of broadening coefficients are calculated for a different collisional  
424 system) we can conclude that for this band our sets of experimental coef-  
425 ficients can be safely compared to isotropic calculated coefficients without  
426 introducing significant errors.

### 427 3. Theoretical part

#### 428 3.1. Potential Energy Surface

429 In the present work, quantum dynamical calculations were performed on  
430 the CO-N<sub>2</sub> potential energy surface of Liu *et al.* [2] already described and  
431 used by some of us in Ref. [34]. The Jacobi coordinates are described in the  
432 two preceding publications. Let us denote the CO and N<sub>2</sub> monomers by the  
433 subscripts  $A$  and  $B$ . The nitrogen molecule bond length is fixed to its ex-  
434 perimental ground state value,  $r_B = 1.100068 \text{ \AA}$  resulting in a 5-dimensional  
435 potential  $V(r_A, R, \theta_A, \theta_B, \phi)$ . This dimension reduction is not a problem in  
436 our case, since N<sub>2</sub> is the perturbing molecule and remains in its vibrational  
437 ground state in a wide range of temperatures relevant for our spectroscopic



438 study. The code provided by Liu *et al.* [2] to generate their PES allows to  
 439 average the PES over the intramolecular CO distance,  $r_A$ . We are thus able  
 440 to consider the CO molecule either in its ground or first excited vibrational  
 441 states. We furthermore denote this average over the CO vibrational wave  
 442 functions  $\chi_v(r_A)$  with  $v = 0$  or 1 by:

$$\langle V(r_A, R, \theta_A, \theta_B, \phi) \rangle_v = \int_0^\infty \chi_v(r_A) V(r_A, R, \theta_A, \theta_B, \phi) \chi_v(r_A) dr_A. \quad (5)$$

443 We therefore neglect the rotational dependence of the CO wave functions, a  
 444 limitation not severe for this molecule in its first rotational states.

445 For computing facilities these two PESs have been developed over bi-  
 446 spherical harmonics:

$$\langle V(r_A, R, \theta_A, \theta_B, \phi) \rangle_v = \sum_{L_A, L_B, L} \langle V_{L_A, L_B, L}(r_A, R) \rangle_v I_{L_A, L_B, L}(\theta_A, \theta_B, \phi). \quad (6)$$

447 The angular functions are expressed in terms of spherical harmonics tied to  
 448 the CO and N<sub>2</sub> monomers [34, 45, 62–64]:

$$I_{L_A, L_B, L}(\theta_A, \theta_B, \phi = \phi_A - \phi_B) = \sqrt{\frac{2L+1}{4\pi}} \times \sum_m (L_A m L_B - m | L_A L_B L 0) Y_{L_A, m}(\theta_A, \phi_A) Y_{L_B, -m}(\theta_B, \phi_B), \quad (7)$$

449 where (...|...) are Clebsch-Gordan coefficients and  $|m| \leq \min(L_A, L_B)$ . For  
 450 computing reasons<sup>1</sup> we have retained 94 potential radial coupling terms for  
 451 both vibrational states,  $\langle V_{L_A, L_B, L}(r_A, R) \rangle_v$ , with  $L_A = 0, 1, \dots, 10$ ,  $L_B =$   
 452  $0, 2, \dots, 8$ ,  $|L_A - L_B| \leq L \leq L_A + L_B$  and  $L_A + L_B + L$  even. Following Green  
 453 [65, 66] and MOLSCAT [67] idiosyncratic normalisation, the radial terms  
 454 were obtained via Gauss-Legendre quadratures over the  $\theta$ 's and a Chebyshev  
 455 quadrature over  $\phi$ :

---

<sup>1</sup>Close coupling calculations are very time consuming and moreover we encountered memory size problems using more terms in this expansion

$$\begin{aligned}
& \langle V_{L_A, L_B, L}(r_A, R) \rangle_v = \frac{8\pi^2}{2L+1} \\
& \times \int_0^{2\pi} d\phi \int_{-1}^{+1} d(\cos\theta_A) \int_{-1}^{+1} d(\cos\theta_B) \langle V(r_A, R, \theta_A, \theta_B, \phi) \rangle_v I_{L_A, L_B, L}(\theta_A, \theta_B, \phi).
\end{aligned}
\tag{8}$$

456 The first radial coupling terms are presented in Fig. 2 of Ref. [34] They were  
457 generated on a regular grid from 4 to 200 bohrs with a constant step size of  
458 0.2 bohrs.

### 459 3.2. Quantum dynamical methods

460 In order to obtain scattering matrix elements to derive the line shape pa-  
461 rameters (see below) we have used (for historical reasons) both the MOLSCAT  
462 code 14 [67] and the version recently published by Hutson and Le Sueur [68].  
463 The close coupling (CC) method is the most accurate but unfortunately also  
464 the most time consuming. For the present system, as already discussed by  
465 Józwiak et al. [34] such calculations are not easy to carry<sup>2</sup> despite the or-  
466 tho/para disparity in nitrogen that allows us to perform separate calculations  
467 for CO-oN<sub>2</sub> and CO-pN<sub>2</sub>. Neglecting any vibrational coupling terms we have  
468 performed four sets of calculations: two for CO-oN<sub>2</sub> or -pN<sub>2</sub> with the CO  
469 molecule in either v= 0 or v= 1. Close coupling calculations were performed  
470 for total energies from 0.1 cm<sup>-1</sup> to a maximum of 300 cm<sup>-1</sup> and the coupled  
471 states approximation (CSA) was used up to 506 cm<sup>-1</sup>. Above this energy  
472 even the CSA is too time consuming. Readers interested in the CSA may  
473 consult Ref. [34] and references therein. The necessary generalized cross  
474 sections to compute the line shape parameters were obtained by different  
475 methods described in the next sections.

### 476 3.3. Generalized Cross sections

477 Following the pioneering work of Hess [69], the so-called generalized Hess  
478 method (GHM) provides the spectroscopic cross sections [70, 71] for a spec-  
479 troscopically active diatomic molecule in a bath of diatomic molecules:

---

<sup>2</sup>As an example, for CO-oN<sub>2</sub> at a total energy of 300 cm<sup>-1</sup> with a basis of 417 triplets ( $j_1, j_2, j_{12}$ ) and a total angular momentum  $J = 100$ , the number of open channels ( $j_1, j_2, j_{12}, l$ ) is 3050.

$$\begin{aligned}
\sigma_{\lambda}^{(q)}(v_i j'_i, v_f j'_f; v_i j_i, v_f j_f; j_2, j'_2; E_{kin}) &= \frac{\pi}{k^2} (-1)^{(\lambda+j_f-j'_f+j_2-j'_2)} \left( \frac{[j'_i]}{[j_i]} \right)^{1/2} \\
&\times \sum_{\ell, \ell', \bar{\ell}, \bar{\ell}'} ([\ell] [\ell'] [\bar{\ell}] [\bar{\ell}'])^{1/2} i^{(\ell-\ell'-\bar{\ell}+\bar{\ell}')} (-1)^{\ell'-\bar{\ell}'} \begin{pmatrix} \ell & \bar{\ell} & \lambda \\ 0 & 0 & 0 \end{pmatrix} \begin{pmatrix} \ell' & \bar{\ell}' & \lambda \\ 0 & 0 & 0 \end{pmatrix} \\
&\times \sum_{J, \bar{J}} [J] [\bar{J}] \sum_{L, L', \bar{L}, \bar{L}'} ([L] [L'] [\bar{L}] [\bar{L}'])^{1/2} \begin{Bmatrix} \lambda & \bar{\ell} & \ell' \\ j'_2 & L' & \bar{L}' \end{Bmatrix} \begin{Bmatrix} \lambda & \bar{\ell} & \ell \\ j_2 & L & \bar{L} \end{Bmatrix} \begin{bmatrix} L & L' & j_f & j'_f \\ \bar{L} & j_i & \bar{L}' & j_i \\ \lambda & \bar{J} & J & q \end{bmatrix} \\
&\times \left[ \delta_{j_i j'_i} \delta_{j_f j'_f} \delta_{j_2 j'_2} \delta_{\ell \ell'} \delta_{\bar{\ell} \bar{\ell}'} \delta_{L L'} \delta_{\bar{L} \bar{L}'} \right. \\
&\left. - \langle v_i j_i(j_2 \ell) L | S^J(E_{T_{i_2}}) | v_i j'_i(j'_2 \ell') L' \rangle \langle v_f j_f(j_2 \bar{\ell}) \bar{L} | S^{\bar{J}}(E_{T_{f_2}}) | v_f j'_f(j'_2 \bar{\ell}') \bar{L}' \rangle^* \right]. \tag{9}
\end{aligned}$$

480 S-matrix elements are evaluated at the the total energies  $E_{T_{i_2}} = E_{kin} +$   
481  $E_{v_i j_i} + E_{j_2}$  and  $E_{T_{f_2}} = E_{kin} + E_{v_f j_f} + E_{j_2}$ .  $k$  is the modulus of the wave  
482 vector associated with the relative collisional energy,  $E_{kin} = (\hbar k)^2/2\mu$ , with  
483  $\mu$  the reduced mass of the CO-N<sub>2</sub> system. These cross sections are expressed  
484 in Å<sup>2</sup> [72–74]. The vibrational quantum number  $v_2$  has been omitted since it  
485 is always 0 in our case for the nitrogen molecule. In Eq. (9), primes indicate  
486 post-collisional values,  $v_i j_i, v_f j_f$  designates a CO optical transition (denoted  
487  $|l\rangle$ ) later on) and  $v_i j'_i, v_f j'_f$  a line ( $|l'\rangle$ ) later on) to which the line  $|l\rangle$  is  
488 coupled by collisions.  $q$  designates the line type ( $q = 0$  for an isotropic Raman  
489 transition,  $q = 1$  for an electric dipole transition,  $q = 2$  for an anisotropic  
490 Raman transition). The coupling scheme is  $\vec{j}_2 + \vec{\ell} = \vec{L}$ , which in turn is  
491 coupled to the rotational angular momentum of the active molecule,  $\vec{j}_i$ , to  
492 give the total angular momentum  $\vec{J}$ . [X] stands for  $2X+1$ , ( $: : :$ ) refers  
493 to the 3-j symbol and  $\begin{bmatrix} : & : & : \\ : & : & : \end{bmatrix}$  to the 12-j symbol of the second kind [75].  
494 Equation (9) leads to two kinds of cross-sections depending on the  $\lambda$  value,  
495 the rank of the velocity of the active molecule. For  $\lambda = 0$  one recovers  
496 [70–72, 76, 77] the standard generalized spectroscopic cross section [48, 49]  
497 leading to the relaxation matrix [78, 79]. **The simplified expression of Eq. (9)**  
498 **for the diagonal cross sections (pressure broadening and shift) is given by**  
499 **equations 4-6 of Ref. [80] in the case of isotropic Raman Q lines.** The  $\lambda = 1$   
500 value is associated with velocity-changing collisions. **Finally, Eq. (9) is valid**

501 whatever the kind of the optical transition and allows the calculations of  
 502 both the diagonal and off-diagonal cross sections. Since in the present study  
 503 we are dealing with the Q lines in Eq. (9) we have  $j_i = j_f$  and  $j_{i'} = j_{f'}$  as  
 504 well.

505 Starting from Eq. (9), specialized to the Q(0) line for which  $j_i = j_f = 0$ ,  
 506  $v_i = 0$  and  $v_f = 1$ , we have performed a full CC calculations using our GHM  
 507 code [81] to determine the diagonal cross sections in the cases  $\lambda=0$  and  $\lambda=1$   
 508 (note that in MOLSCAT codes the calculation of such cross sections is not  
 509 implemented). Because the present experiment cannot allow to see the effects  
 510 of the velocity-changing collisions, tied to  $\lambda=1$ , on the spectral line shapes,  
 511 the theoretical velocity changing collision frequencies are only presented in  
 512 Appendix A. The exact pressure broadening coefficients obtained by this  
 513 method are also provided in this Appendix.

514 As stated above, for  $\lambda = 0$  the real part of the diagonal ( $|l\rangle\rangle = |l'\rangle\rangle$ )  
 515 cross section is the pressure broadening cross sections which includes two  
 516 contributions, one coming from elastic collisions and one coming from the  
 517 inelastic ones for the active molecule [79, 80, 82–84]. The neglect of the first  
 518 contribution leads to the so-called random phase approximation (RPA):

$$\begin{aligned} \sigma_0^{(q)}(v_i j_i, v_f j_f; v_i j_i, v_f j_f; j_2 j_2') = \\ = \frac{1}{2} \left\{ \sum_{j_1 \neq j_i} \sigma(v_i j_i j_2 \rightarrow v_i j_1 j_2') + \sum_{j_1 \neq j_f} \sigma(v_f j_f j_2 \rightarrow v_f j_1 j_2') \right\}. \end{aligned} \quad (10)$$

519 We furthermore define a partial pressure broadening cross section as

$$\sigma_0^{(q)}(j_i, j_f; j_i, j_f; j_2) = \sum_{j_2'} \sigma_0^{(q)}(j_i, j_f; j_i, j_f; j_2, j_2') \quad (11)$$

520 whatever the method used for determining it (we have dropped the v's for  
 521 short). Figures 9 and 10 provide examples of such partial cross sections for  
 522 the Q(0) and Q(6) lines of the fundamental CO band. One can check that the  
 523 RPA is accurate for kinetic energies larger than about  $50 \text{ cm}^{-1}$ , and that the  
 524 summations of bi-states to bi-states ordinary cross sections are very similar  
 525 in both vibrational states ( $v = 0$  and  $1$ ). The first fact is related to the  
 526 predominant importance of the inelastic collisions for this system, at least  
 527 for kinetic energies larger than  $\sim 50 \text{ cm}^{-1}$ , as it is for comparable ones (e.g.  
 528 CO-Ar [47], CO<sub>2</sub>-He [85] or -Ar [86]). The second observation is due to the

529 fact that the vibrationally averaged PESs in  $v = 0$  and in  $v = 1$  are very  
530 similar and that the rovibrational energy levels spacing is very close in both  
531 CO vibrational states. Moreover, these figures show that the CSA is quite  
532 good, as expected as the kinetic energy and  $j_2$  increase. In addition, even if it  
533 is not obvious from these figures, these partial cross sections are very similar  
534 as  $j_2$  increases; this point has been extensively discussed for this system in  
535 Ref. [34] (see Fig. 6 therein) and shown in previous works ( $\text{N}_2\text{-H}_2$  [62],  $\text{C}_2\text{H}_2$   
536  $\text{-H}_2\text{-D}_2$  [45, 87],  $\text{C}_2\text{H}_2\text{-N}_2$  [64] and  $\text{N}_2\text{-N}_2$  [43]). Consequently, for  $j_2 > 7$  we  
537 have set the partial pressure broadening cross section (Eq. (11)) equal to a  
538 weighted sum of ortho and para contributions determined for  $j_2 \leq 7$ .

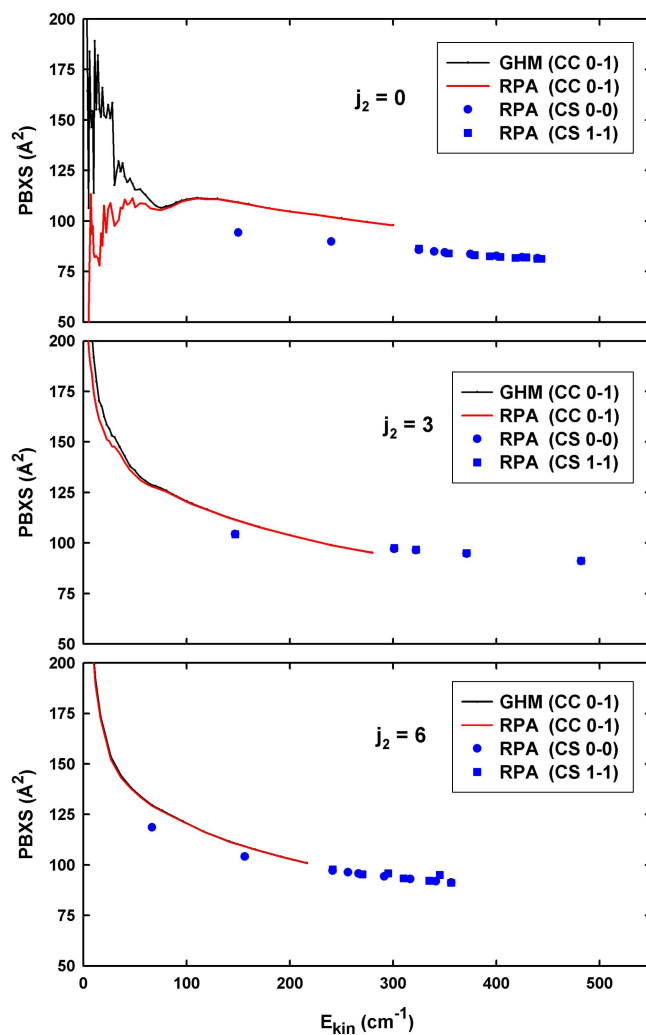


Figure 9: Partial pressure broadening cross sections, as a function of the kinetic energy, for the Q(0) line and  $j_2 = 0, 3$  and  $6$ . The black line is the result of our GHM code [81], this is the most exact calculation; red lines are the CC results of the RPA (see text); blue squares and disks are the results of our CSA calculations either in  $v=0$  or in  $v=1$  [88]

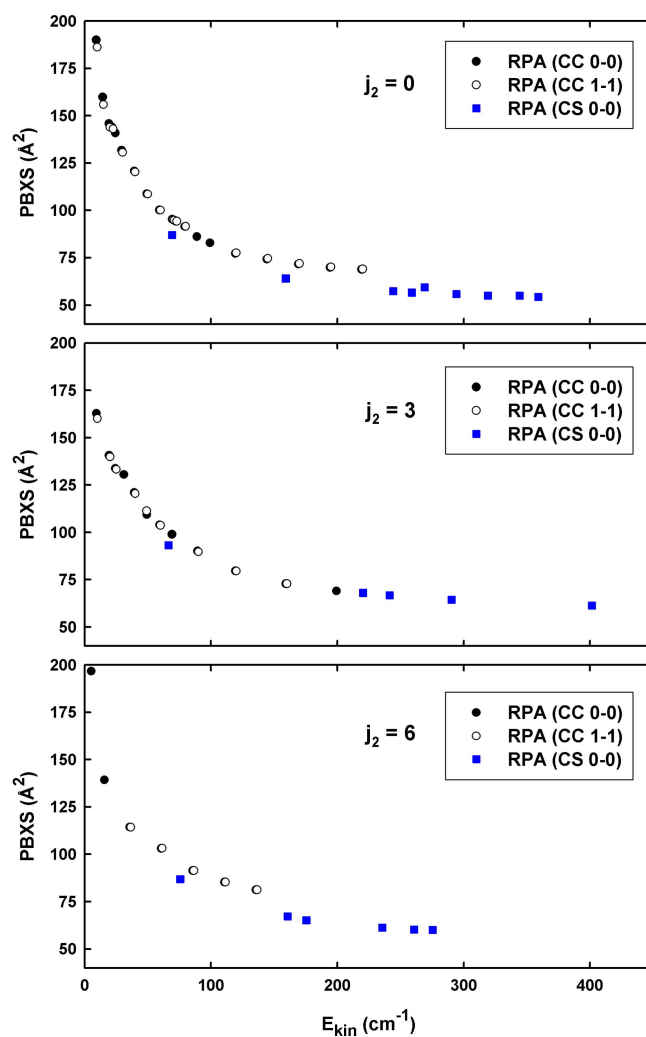


Figure 10: Partial pressure broadening cross sections, as a function of the kinetic energy, for the Q(6) line and  $j_2 = 0, 3$  and 6. The black disks result from bi-states to bi-states CC XS in  $v=0$ ; black circles result from bi-states to bi-states CC XS in  $v=1$ ; blue squares are the results of our CSA calculations in  $v=0$ .

539 *3.4. Relaxation matrix elements*

540 In order to compare the results of our calculations with experimental val-  
 541 ues we formally construct, within the impact approximation, the relaxation  
 542 matrix  $W_{l'l}$  elements [48, 49, 78, 79]:

$$\langle\langle l' | W^{(q)} | l \rangle\rangle = \frac{n \bar{v}_r}{2\pi c} \langle \sigma_0^{(q)}(l', l; E_{kin}) \rangle \quad (12)$$

543 where  $n$  is the ( $N_2$ ) density number (assuming that self perturbation is negli-  
 544 gible),  $\bar{v}_r$  the mean relative speed at the temperature  $T$ , and the denominator  
 545 converts angular frequency to wavenumber (in  $\text{cm}^{-1}$  with the speed of light  $c$   
 546 expressed in  $\text{cm/s}$ ). The thermally averaged cross sections over the Maxwell-  
 547 Boltzmann distribution kinetic energies being given by

$$\langle \sigma_0^{(q)}(l', l; E_{kin}) \rangle = \sum_{j_2} \rho(j_2) \langle \sigma_0^{(q)}(j'_i, j'_f; j_i, j_f; j_2; E_{kin}) \rangle, \quad (13)$$

548 with the thermally averaged partial cross section

$$\begin{aligned} \langle \sigma_0^{(q)}(j'_i, j'_f; j_i, j_f; j_2; E_{kin}) \rangle &= \\ &= \frac{1}{(k_B T)^2} \int_0^\infty E_{kin} e^{-E_{kin}/k_B T} \sigma_0^{(q)}(j'_i, j'_f; j_i, j_f; j_2; E_{kin}) dE_{kin} \end{aligned} \quad (14)$$

549 and the thermal equilibrium populations given by

$$\rho(j_2) = w_{j_2} (2j_2 + 1) \exp(-E_{j_2}/k_B T) / Z(T). \quad (15)$$

550 The nuclear spin weights  $w_{j_2}$  are equal to  $2/3$  for  $oN_2$  and  $1/3$  for  $pN_2$ ;  
 551  $Z(T)$  is the rotational partition function. Making use of our GHM code  
 552 [81] we have all the necessary equations to generate the pressure broadening  
 553 coefficients  $\gamma_l = W_l^{(0)}$  for the Q(0) line of the fundamental band of CO at  
 554 various temperatures. For the other lines (as well also for the Q(0) line for  
 555 comparison) we made use of the CC and CSA bi-state to bi-state ordinary  
 556 cross sections. Therefore a few more equations are needed.

557 For (hypothetical) isotropic Raman lines in a fixed vibrational states a  
 558 generalized spectroscopic cross section is exactly a **negated** state to state  
 559 cross section [48, 66]:

$$\sigma_0^{(0)}(j'_1 j'_1; j_1 j_1; j_2 j'_2; E_{kin}) = -\sigma(j_1 j_2 \rightarrow j'_1 j'_2; E_{kin}). \quad (16)$$



560 Moreover, the sum rule is exact [48, 49, 66] leading to the expression of the  
 561 diagonal relaxation matrix elements in terms of the off-diagonal ones:

$$W_l^{(0)} = - \sum_{l' \neq l} W_{l'}^{(0)}. \quad (17)$$

562 The off-diagonal terms being simply a weighted sum of standard rate con-  
 563 stants:

$$W_{l'}^{(0)} = - \sum_{j_1 j_2 \rightarrow j_1' j_2'} \rho(j_2) R(j_1 j_2 \rightarrow j_1' j_2'). \quad (18)$$

564 We are now in position to apply the RPA using our CC and CSA rates:

$$\begin{aligned} \gamma_l &= \langle\langle l | W^{(q)} | l \rangle\rangle = \langle\langle v_i j_i v_f j_f | W^{(q)} | v_i j_i v_f j_f \rangle\rangle = \\ &= \frac{1}{2} \{ \langle\langle v_i j_i v_f j_i | W^{(0)} | v_i j_i v_f j_i \rangle\rangle + \langle\langle v_i j_f v_f j_f | W^{(0)} | v_i j_f v_f j_f \rangle\rangle \}. \end{aligned} \quad (19)$$

565 Note that we have considered that Eq. (19) holds whatever the order of  
 566 the radiation-mater interaction,  $q$ , which is the essence of the RPA. Because  
 567 the state to state cross sections in  $v = 0$  and in  $v = 1$  are very close we  
 568 have also performed an average (that is not the RPA) for the off-diagonal  
 569 relaxation matrix elements:

$$\begin{aligned} \langle\langle l' | W^{(0)} | l \rangle\rangle &= \frac{1}{2} \{ \langle\langle v_i j_i' v_i j_f' | W^{(0)} | v_i j_i v_i j_f \rangle\rangle \\ &\quad + \langle\langle v_f j_i' v_f j_f' | W^{(0)} | v_f j_i v_f j_f \rangle\rangle \}. \end{aligned} \quad (20)$$

570 This allows us to define an averaged line mixing parameter [48, 49, 53, 54,  
 571 89, 90] for isotropic Raman Q lines of the fundamental band:

$$Y_{l;0-1\text{band}} = \frac{1}{2} \{ Y_{l;v=0} + Y_{l;v=1} \} \quad (21)$$

572 with

$$Y_{l;v} = 2 \sum_{l' \neq l} \frac{W_{l'l;v}}{\sigma_l - \sigma_{l'}} \quad (22)$$

573 where  $\sigma_i$  is the line position. Because a relaxation matrix element  $W_{\nu l, \nu}$  is  
574 derived from rate constants in a given vibrational level, any imaginary part  
575 is neglected.

### 576 3.5. Theoretical coefficients

577 Due to our limited grid in kinetic energies, up to  $300 \text{ cm}^{-1}$  and  $506 \text{ cm}^{-1}$   
578 for our CC and CSA calculations respectively, in order to perform the thermal  
579 average (Eq. 14), the cross sections were extrapolated up to  $2000 \text{ cm}^{-1}$  using  
580 a polynomial form in  $a+b/E_{kin}$ , where  $a$  and  $b$  are fitted constants. Therefore  
581 our mixed CC/CSA calculations are mainly CC results below 100 K and more  
582 affected by the CSA calculations and this extrapolation at 300 K.

583 First we come back to the Q(0) line of the fundamental band and discuss  
584 its pressure broadening coefficients at various temperatures. Figure 11 com-  
585 pares 3 kinds of calculations. As compared to our "exact" GHM calculations  
586 this figures shows that the RPA values obtained from our CC set are very  
587 good even at the lowest temperature (50 K). Our RPA values deduced from  
588 our mixed set of CC/CSA cross sections are in very good agreement with the  
589 GHM values except at 50 K for which the agreement is nonetheless not bad.  
590 A provides the GHM parameters for the Q(0) line and the table therein shows  
591 the detailed comparison for the HWHM determined with the RPA and the  
592 GHM. Note that the sum rule, Eq. (17), is verified to better than 5% with  
593 our exact GHM coefficients. Recall that the RPA is expected to work better  
594 as  $T$  and  $j$  increase [83, 85, 86, 91]. Therefore, we conclude that our RPA  
595 deduced from our CC/CSA calculations should be quite accurate between 50  
596 and 300 K for all the studied lines. Figure 12 displays such results for the  
597 Q( $j = 0 - 6$ ) lines.

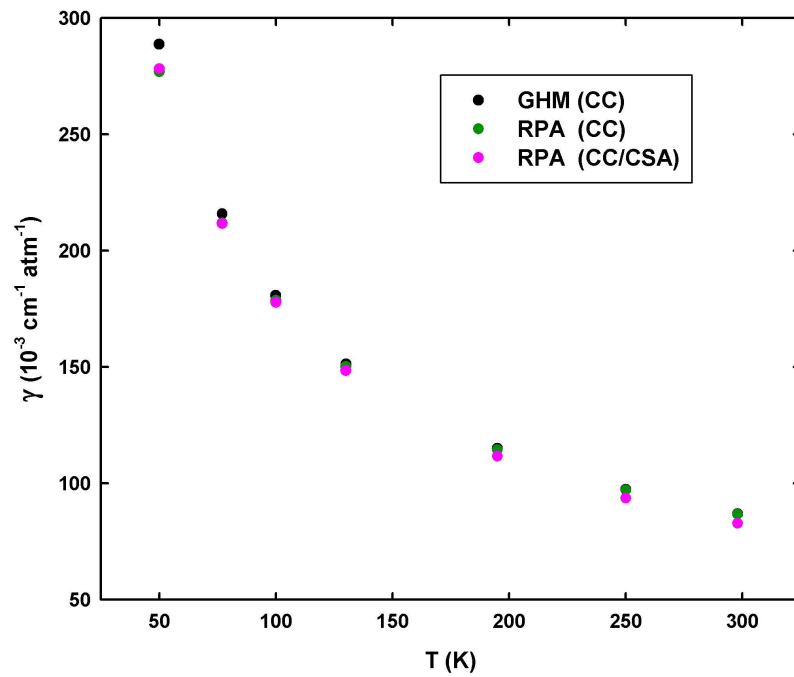


Figure 11: Pressure broadening coefficients at selected temperatures for the Q(0) line of the 0-1 band using the generalized Hess method, the random phase approximation from our CC rates or mixed CC/CSA rates.

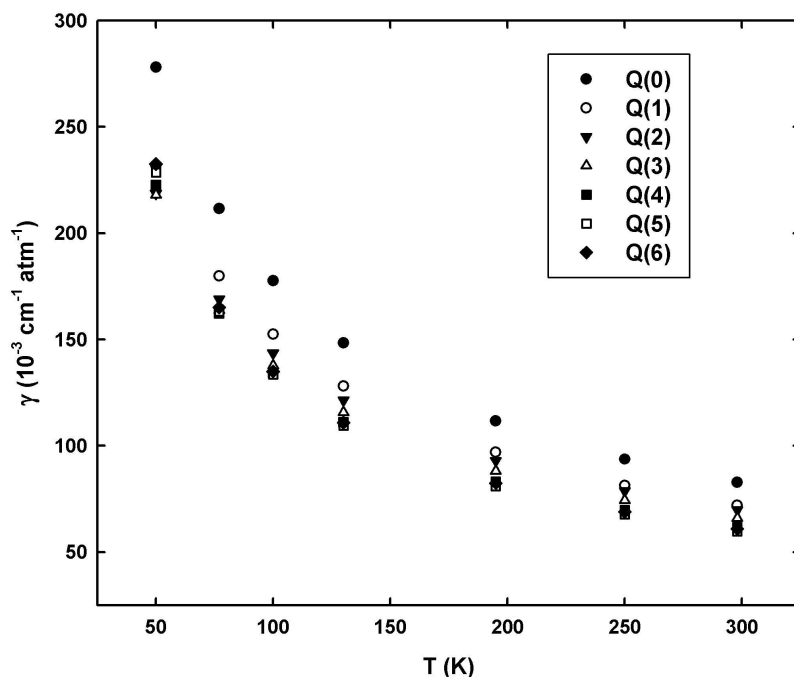


Figure 12: Pressure broadening coefficients at selected temperatures for the Q(0) to Q(6) lines of the fundamental band in N<sub>2</sub> calculated with with our mixed set of CC/CSA rate constants and the RPA.

598 In order to determine the line mixing coefficients for the Q(0) to Q(6)  
 599 isotropic Raman lines we have considered a truncated relaxation matrix in-  
 600 cluding the first 11 lines. Convergence tests show that in fact 90% of a line  
 601 mixing parameter is due to the four neighbouring lines.

602 As an additional work, on the basis of the RPA, we have calculated the in-  
 603 elastic contribution to the pressure broadening coefficient for pure rotational  
 604 Stokes lines and electric dipole R lines. Results are given in B.

#### 605 4. Results and Discussion

606 The main goal of the work presented in this article is the obtention of  
 607 collisional line broadening and line mixing coefficients for isotropic Q-branch  
 608 Raman lines of the fundamental of CO in nitrogen baths at different temper-  
 609 atures. This has been carried out independently from both an experimental  
 610 and a theoretical point of view as described in the preceding sections. The  
 611 final results from both approaches are presented jointly in Tabs. 2 and 3. In

612 order to facilitate their comparison they are also displayed simultaneously in  
613 Figs. 7 (broadening coefficients) and 8 (line mixing coefficients).

614 For the broadening coefficients the results show very good agreement  
615 between experiment and calculation. In fact, the agreement is excellent at  
616 195 K, with nearly all the calculated coefficients within the estimated error  
617 interval of the experimentally determined values. It is still very good at 77  
618 K, with an average deviation between theory and experiment of only 3.25%  
619 (with a maximum of 6.1% for  $j = 2$ ). For 298 K, and if we exclude the  
620 coefficient for  $j = 0$ , whose experimental determination shows a very large  
621 uncertainty, the average deviation between experiment and calculation is  
622 6.4% with a maximum of 10.5% for  $j = 3$ . While not as good as for the other  
623 two temperatures, it is still a satisfactory agreement. From Fig. 7 it is also  
624 clearly visible that the calculated coefficients are generally very close to the  
625 experimental ones for  $j = 0$  (again with the exception of 298 K) and  $j = 6$   
626 but tend to slightly underestimate them for  $j = 1, \dots, 4$ . This is especially  
627 noticeable at 77 and 298 K, since the differences are larger and the pattern  
628 easier to see at these temperatures.

629 The agreement in the line mixing coefficients is also very good, as shown  
630 in Fig. 8. The largest relative differences happen at 77 K for  $j = 3$  and  $j = 4$ .  
631 The origin of the discrepancy is difficult to pinpoint, as it may lie in either the  
632 experimental or theoretical side, or in both of them: from the experimental  
633 side, an accurate experimental determination of line mixing coefficients when  
634 their values get close to zero, as is the case for these lines, pushes the limits of  
635 a technique like SRS, which produces worse S/N ratios than those of typical  
636 IR absorption experiments and can be affected by noises of non-statistical  
637 nature like drifts in laser power or beam alignment.

638 From the calculations point of view, the accuracy of the predicted line  
639 broadening and mixing coefficients is going to be affected by the approxima-  
640 tions used. Namely the use of the random phase approximation, and thus  
641 the neglect of the elastic contributions and of a vibrational phase shift, the  
642 use of a mixed set of CC/CSA rates and the limitation of our grid in kinetic  
643 energies. In particular the neglect of the elastic contributions should lead  
644 to an underestimation of the PB (pressure broadening) coefficients at low  
645 temperatures. Contrarily, our limited grid will affect more our calculated  
646 values as the temperature increases. Despite this, both the calculated pres-  
647 sure broadening and mixing coefficients follow the main trend with both  $j$   
648 and T when compared to the present experimental values. Moreover, the  
649 line mixing parameters compare well to previous evaluations for the same

| $j$ | $\gamma_{\text{HWHM}}$ (77 K) |       | $\gamma_{\text{HWHM}}$ (195 K) |       | $\gamma_{\text{HWHM}}$ (298K) |       |
|-----|-------------------------------|-------|--------------------------------|-------|-------------------------------|-------|
|     | Exp.                          | Calc. | Exp.                           | Calc. | Exp.                          | Calc. |
| 0   | 211(5)                        | 211.5 | 108(6)                         | 111.7 | 51(47)                        | 82.7  |
| 1   | 190(2)                        | 180.0 | 99(6)                          | 96.9  | 79(6)                         | 72.0  |
| 2   | 180(2)                        | 169.0 | 90(3)                          | 93.0  | 73(3)                         | 69.9  |
| 3   | 172(2)                        | 163.8 | 89(2)                          | 88.1  | 74(2)                         | 66.1  |
| 4   | 170(2)                        | 162.3 | 85(1)                          | 83.1  | 67(2)                         | 61.7  |
| 5   | 165(2)                        | 163.1 | 84(1)                          | 81.0  | 63(2)                         | 59.7  |
| 6   | 164(2)                        | 165.0 | 82(1)                          | 82.4  | 60(1)                         | 60.9  |
| 7   | 165(2)                        |       | 81(1)                          |       | 59(1)                         |       |
| 8   | 168(2)                        |       | 80(1)                          |       | 59(1)                         |       |
| 9   | 165(4)                        |       | 80(2)                          |       | 58(2)                         |       |
| 10  | 160(6)                        |       | 79(2)                          |       | 56(2)                         |       |
| 11  | 145(13)                       |       | 76(2)                          |       | 57(2)                         |       |
| 12  |                               |       | 78(3)                          |       | 57(2)                         |       |
| 13  |                               |       | 76(3)                          |       | 54(2)                         |       |
| 14  |                               |       | 74(4)                          |       | 56(2)                         |       |
| 15  |                               |       | 82(11)                         |       | 52(3)                         |       |
| 16  |                               |       |                                |       | 54(3)                         |       |
| 17  |                               |       |                                |       | 55(4)                         |       |
| 18  |                               |       |                                |       | 52(5)                         |       |
| 19  |                               |       |                                |       | 61(8)                         |       |

Table 2: Experimental and calculated collisional broadening coefficients  $\gamma_{\text{HWHM}}$  for the Q branch of the  $v=0 \rightarrow v=1$  band of CO in N<sub>2</sub> at 77, 195 and 298 K. Numbers in parentheses are given in units of the last significant digit and represent 1 standard error. Units are  $10^{-3} \text{ cm}^{-1} \text{ atm}^{-1}$ .

| $j$ | $Y_j^p$ (77 K) |       | $Y_j^p$ (195 K) |       | $Y_j^p$ (298 K) |
|-----|----------------|-------|-----------------|-------|-----------------|
|     | Exp.           | Calc. | Exp.            | Calc. | Calc.           |
| 0   | -4.8(3)        | -4.9  | -2.5(11)        | -2.2  | -1.6            |
| 1   | -1.1(2)        | -1.0  | -0.63(9)        | -0.5  | -0.3            |
| 2   | -0.12(9)       | 0.0   | -0.02(6)        | -0.1  | -0.1            |
| 3   | 0.12(9)        | 0.3   | 0.05(6)         | 0.0   | 0.0             |
| 4   | 0.18(11)       | 0.4   | 0.08(6)         | 0.1   | 0.0             |
| 5   | 0.34(8)        | 0.4   | 0.11(6)         | 0.0   | 0.0             |
| 6   | 0.25(11)       | 0.4   |                 | 0.1   | 0.05            |
| 7   | 0.24(2)        |       |                 |       |                 |
| 8   | 0.1(2)         |       |                 |       |                 |

Table 3: Experimental and calculated Rosenkranz line mixing coefficients  $Y_j^p$  for the Q( $j$ ) lines at 77, 195 and 298 K (calculated only) in the fundamental band of CO in N<sub>2</sub>. Numbers in parentheses are given in units of the last significant digit and represent 1 standard error. Units are atm<sup>-1</sup>.

650 band of CO in helium baths [53]. In view of this, the overall present level  
651 of agreement found between theory and experiment for the line broadening  
652 and mixing coefficients can be considered very satisfactory.

## 653 5. Conclusions

654 The work described throughout this article consists of a joint experimental  
655 and theoretical study of the pressure dependence of the shapes of the spectral  
656 lines in the rovibrational Raman Q-branch of the CO molecule in a bath of  
657 N<sub>2</sub>. Quantitative data on line broadening and mixing in the CO-N<sub>2</sub> collisional  
658 system at temperatures between 77 and 298 K, in the form of broadening and  
659 mixing coefficients, have been obtained in parallel by both the experimental  
660 and theoretical branches of the study. These coefficients and the comparison  
661 between their experimental and calculated values constitute the main result  
662 of this work.

663 From the experimental point of view, the CO-N<sub>2</sub> collisional system had  
664 never before been studied by rovibrational Raman spectroscopy with this  
665 level of instrumental resolution. Furthermore, the few experimental studies  
666 of the system available in the bibliography do not provide broadening or

667 mixing coefficients for this band. We are thus presenting a completely new  
668 and valuable experimental data set from which future studies using Raman  
669 spectroscopy can benefit.

670 From the theoretical point of view, this is also the first time that ad-  
671 vanced, quantum dynamical calculations are used to obtain broadening and  
672 mixing data on this Raman band in the CO-N<sub>2</sub> collisional system, since pre-  
673 vious studies made use of semiempirical methods. The advanced calculation  
674 methodology has been coupled with the use of a very modern, state-of-the-art  
675 PES. The very good agreement found between our experimental and theo-  
676 retical results is a robust indication of the accuracy of the methodologies  
677 used and, especially, of the reliability of the data sets obtained. The results  
678 presented here might also be considered as yet another validation of the PES  
679 of Liu et al. [2].

680 Regarding the potential impact of our results, the CO-N<sub>2</sub> collisional sys-  
681 tem is present in a number of different fields, as reviewed in the introduction.  
682 Future studies in these fields can benefit from our data. Any measurements  
683 using rovibrational Raman spectroscopy (typically CARS) to determine the  
684 concentration of CO in a CO-N<sub>2</sub> mixture can use our broadening and mixing  
685 coefficients to this end. In the case of combustion studies, which generally  
686 take place at higher temperatures than the ones covered in this study, the  
687 fact that our data have been obtained at several temperatures can be used  
688 for an extrapolation of the coefficients to the region of interest using the  
689 well-known temperature power law for the pressure broadening coefficients

690 The knowledge of broadening and line mixing coefficients is also necessary  
691 for an adequate modeling of planetary atmospheres, both terrestrial and of  
692 other bodies, in which the presence of CO and N<sub>2</sub> has been detected. Since  
693 most atmospheric and astrophysical spectroscopic measurements are carried  
694 out by means of absorption techniques (infrared or microwave), the additional  
695 theoretical values reported for the pure rotational R- and S- lines might be  
696 of particular importance. For instance, the results reported here can be used  
697 as initial parameters in a fit of experimental spectra (both pure rotational  
698 and, due to a small contribution from the rovibrational phase-shift, of the  
699 fundamental band).

700 Finally, the values we have determined may be also used as a reference  
701 data for future theoretical studies of line-shape parameters of rovibrational  
702 transitions.



703 **6. Acknowledgement**

704 D. Paredes-Roibás and R. Z. Martínez acknowledge the funding received  
 705 from Project FIS2017-84391-C2-1-P of Ministerio de Economía y Competi-  
 706 titividad. H. Józwiak’s contribution is supported by the National Science  
 707 Centre in Poland through Project No. 2018/31/B/ST2/00720.

708 **A. Additional close coupling line shape parameters for the Q(0)**  
 709 **line**

710 In this first appendix we provide the line shape parameters, excluding the  
 711 line mixing one, at various temperatures for the Q(0) line as deduced from  
 712 our close coupling calculations and the GHM method. We remind the reader  
 713 that the frequency of the velocity changing collisions leading to the Dicke  
 714 narrowing are given by [73, 74, 92, 93]:

$$\tilde{\nu}_{opt} \equiv \tilde{\omega}_R - \tilde{\omega}_A. \quad (S1)$$

715 In Hess notations [69, 71]  $\tilde{\omega}_A \equiv \tilde{\omega}_0^{00}(q)$  is nothing else but the complex diag-  
 716 onal relaxation matrix element  $(\gamma - i\delta)$  and the relaxation frequency  $\tilde{\omega}_R$  is  
 717 linked to the combined effect of the translational and internal motions. It is  
 718 expressed in terms of two, mass weighted, collision integrals:

$$\tilde{\omega}_R = n_b \frac{m_a}{m_a + m_b} \tilde{\omega}_0^{00}(q) + \frac{2}{3} n_b \frac{m_b}{m_a + m_b} \tilde{\omega}_1^{11}(q), \quad (S2)$$

719 where  $m_a$  is the mass of the optically active molecule (CO) and  $m_b$  the mass  
 720 of the perturber (N<sub>2</sub>). The collision integrals [94] are derived from the GHM  
 721 cross sections (Eq. (8)):

$$\tilde{\omega}_\lambda^{s,s'}(q) = \bar{v}_r \int dx x^{(s+s'+2)/2} e^{-x} \sigma_\lambda^{(q)}(E_{kin} = xk_B T). \quad (S3)$$

722 Table 4 gathers the line shape parameters as provided by the GHM  
 723 method for the Q(0) line of the fundamental of CO in N<sub>2</sub>. One can see  
 724 that the RPA slightly underestimates the actual PB coefficients, especially  
 725 at the lowest temperatures. **Moreover, the magnitude of the line shift, due to**  
 726 **the difference of the crossed products of elastic scattering amplitudes in the**  
 727 **ground and excited vibrational states (equation 6a of Ref. [80]), is smaller**  
 728 **than 5% of the PB coefficients, justifying a posteriori their neglect in the**  
 729 **experimental work.** Finally, the effect of the velocity changing collisions has

730 been disregarded in the experimental spectra but Table 4 shows that in fact  
 731 the real part of the complex Dicke parameter is not negligible (for comparison  
 732 with a similar system, CO in argon baths, see Ref. [95]).

Table 4: Line shape parameters for the Raman Q(0) line of the fundamental band of CO in N<sub>2</sub>, in 10<sup>-3</sup> cm<sup>-1</sup> atm<sup>-1</sup>, and for selected temperatures: pressure broadening coefficients ( $\gamma_0$ ) (and the RPA value), pressure shift coefficients ( $\delta_0$ ), real and imaginary parts of the complex Dicke parameter ( $\tilde{\nu}_{opt}$ ).

| T(K) | RPA   | $\gamma_0$ | $\delta_0$ | $\tilde{\nu}_{opt}^r$ | $\tilde{\nu}_{opt}^i$ |
|------|-------|------------|------------|-----------------------|-----------------------|
| 50   | 276.9 | 288.7      | -13.4      | 46.9                  | 4.8                   |
| 77   | 211.8 | 215.9      | -6.9       | 31.4                  | 1.8                   |
| 100  | 178.7 | 180.8      | -4.9       | 25.0                  | 1.0                   |
| 130  | 150.1 | 151.3      | -3.5       | 20.2                  | 0.5                   |
| 195  | 114.5 | 114.9      | -2.3       | 15.2                  | 0.1                   |
| 250  | 97.1  | 97.4       | -1.9       | 13.2                  | 0.0                   |
| 298  | 86.6  | 86.8       | -1.6       | 12.0                  | 0.0                   |

## 733 B. Pressure broadening coefficients for S and R lines

734 In this second appendix we provide the inelastic contributions to the pres-  
 735 sure broadening coefficients, at 77, 195 and 298 K, for the first pure rotational  
 736 Stokes and R lines. These values are obtained from our mixed CC/CSA set  
 737 of rate constants used in conjunction with the random phase approximation  
 738 (Eq. (18)). It is well know that if vibration and rotation-vibration interac-  
 739 tion is neglected (i.e. in a rigid rotor approximation) the collisional width  
 740 of an isotropic Raman line is exactly given by inelastic events. For R and S  
 741 lines, in addition to the inelastic contribution, the elastic events come into  
 742 play through reorienting collisions. Such data for R lines **are** obviously in-  
 743 teresting for remote sensing of the atmosphere, while the HWHM of pure  
 744 rotational S lines may be of interest for the study of combustion processes.  
 745 Our data, considered as primary pressure broadening coefficients, **are** not  
 746 expected to be highly accurate, but may serve as initial parameters in a fit of  
 747 experimental spectra. One may also use **them** to guess the temperature de-  
 748 pendence of the pressure broadening coefficients essentially between 195 and  
 749 300 K. Finally, note that the inelastic contributions are roughly the same (to

750 about a few percent) for lines of the fundamental band because of the weak  
 751 vibrational dependence of the PES and a small change of the CO rotational  
 752 constant in the excited vibrational state. However, for the fundamental band  
 753 of CO the vibrational dependence of the interaction potential will induce an  
 754 additional elastic rovibrational dephasing contribution through the S-matrix  
 755 elements involved in the expression of the generalized spectroscopic cross sec-  
 756 tion (Eq. (9)). Nevertheless, this contribution is expected to be quite small  
 757 above room temperature, as is the reorientational contribution (the latter  
 758 being more true as  $j$  increases).

759 Table 5 provides the results for Raman S lines. Unfortunately, we are not  
 760 aware of experimental measurements to compare with, although we note that  
 761 Hsu et al. [36] reported the data for the pure rotational S(6-15) lines. Table 6  
 762 provides our results for R lines. They are compared with experimental values  
 763 available in the literature for the pure rotational R(0), [26–29] R(1), [29, 30]  
 764 R(2) [29, 31] and R(4) [32, 33] lines and with our CSA calculations from  
 765 the previous work [34]. In the latter case, we refer to the values of  $\gamma_0$  and  
 766  $\gamma^\dagger$  (collisional width which includes the effect of speed-dependence of the  
 767 broadening, see Sec. IV in Ref. [34]), obtained from the PES of Liu et al. [2].  
 768 Values of the pressure broadening coefficients at 195 K were determined from  
 769 Refs. [26–28, 30, 31, 34] using the power-law dependence of  $\gamma_0(T)$ . We note  
 770 that the values from Refs. [29] and [33] are reported for the  $^{13}\text{CO}$  molecule,  
 771 although, as pointed out by the authors, the dependence of collisional width  
 772 on the isotope of carbon is negligible. Lack of isotopic dependence in the  
 773 pressure broadening coefficients was also observed for the self-broadened OCS  
 774 lines [29], as well as for the Ar-perturbed lines of CO [96] and He-perturbed  
 775 lines of  $\text{CO}_2$  [97]. Our results also compare quite well with measurements  
 776 performed in the fundamental band [20–23] and even in the first and second  
 777 overtones [24, 25].

Table 5: Inelastic contribution to the pressure broadening coefficients, in  $10^{-3} \text{ cm}^{-1} \text{ atm}^{-1}$ , for the rotational S(0) to S(4) lines of CO in  $\text{N}_2$  at selected temperatures.

| T(K) | S(0)  | S(1)  | S(2)  | S(3)  | S(4)  |
|------|-------|-------|-------|-------|-------|
| 77   | 190.0 | 171.8 | 165.6 | 163.3 | 163.3 |
| 195  | 102.7 | 93.1  | 88.2  | 84.3  | 82.0  |
| 298  | 76.8  | 69.7  | 65.9  | 62.7  | 60.6  |

778 Finally, our calculated values for Q and R lines agree quite well with the

779 most recent extensive calculations [38] performed on the basis of the semi-  
780 classical Robert-Bonamy formalism using a semi-empirical PES, the isotropic  
781 part of which was adjusted to match experimental data. These authors have  
782 shown that, at room temperature, the elastic reorientational contribution to  
783 the linewidth of the S (and thus R) lines is smaller than  $3 \times 10^{-3} \text{cm}^{-1} \text{atm}^{-1}$   
784 for  $j < 4$  and smaller than  $1 \times 10^{-3} \text{cm}^{-1} \text{atm}^{-1}$  for higher  $j$ 's, thus justifying the  
785 RPA.

Table 6: Inelastic contribution to the pressure broadening coefficients, in  $10^{-3} \text{ cm}^{-1} \text{ atm}^{-1}$ , for the rotational R(0) to R(5) lines of CO in  $\text{N}_2$  and a comparison with the experimental data at selected temperatures.

| T(K) |                      | R(0)   | R(1)  | R(2)  | R(3)  | R(4)  | R(5)  |
|------|----------------------|--------|-------|-------|-------|-------|-------|
| 77   | This work            | 195.6  | 174.4 | 166.2 | 163.0 | 162.6 | 163.6 |
| 195  | This work            | 105.6  | 95.5  | 90.1  | 85.8  | 82.3  | 80.5  |
|      | Ref. 26              | 104.2  |       |       |       |       |       |
|      | Ref. 27              | 119.7  |       |       |       |       |       |
|      | Ref. 28              | 109.06 |       |       |       |       |       |
|      | Ref. 30              |        | 104.9 |       |       |       |       |
|      | Ref. 31              |        |       | 101.7 |       |       |       |
|      | Ref. 34              | 117.98 |       |       |       |       |       |
|      | Ref. 34 <sup>a</sup> | 112.82 |       |       |       |       |       |
| 298  | This work            | 78.9   | 71.8  | 67.8  | 64.1  | 61.1  | 60.3  |
|      | Ref. 26              | 76.2   |       |       |       |       |       |
|      | Ref. 27              | 83.1   |       |       |       |       |       |
|      | Ref. 28              | 79.70  |       |       |       |       |       |
|      | Ref. 29 <sup>b</sup> | 78.80  | 73.45 | 69.65 | 68.90 |       |       |
|      | Ref. 30              |        | 76.6  |       |       |       |       |
|      | Ref. 31              |        |       | 71.14 |       |       |       |
|      | Ref. 32 <sup>c</sup> |        |       |       |       | 66.1  |       |
|      | Ref. 33 <sup>b</sup> |        |       |       |       | 64.0  |       |
|      | Ref. 34              | 87.31  |       |       |       |       |       |
|      | Ref. 34 <sup>a</sup> | 83.49  |       |       |       |       |       |

<sup>a</sup>Calculations including the speed-dependence of the broadening.

<sup>b</sup>Measurements performed for  $^{13}\text{CO}$  at  $T = 296 \text{ K}$ .

<sup>c</sup>Measurements performed at  $T = 295 \text{ K}$ .

786 **References**

- 787 [1] M. H. Karimi-Jafari, A. Maghari, A. Farjammnia, Intermolecular po-  
788 tential energy surface of the N<sub>2</sub>-CO dimer: Ab initio investigation and  
789 analytical representation, *J. Phys. Chem. A* 115 (2011) 1143–1151.
- 790 [2] J.-M. Liu, Y. Zhai, X.-L. Zhang, H. Li, Intermolecular configurations  
791 dominated by quadrupole-quadrupole electrostatic interactions: explicit  
792 correlation treatment of the five-dimensional potential energy surface  
793 and infrared spectra for the CO-N<sub>2</sub> complex, *Phys. Chem. Chem. Phys.*  
794 20 (2018) 2036–2047.
- 795 [3] L. A. Surin, I. V. Tarabukin, S. Schlemmer, Y. N. Kalugina, A. van der  
796 Avoird, *Ab initio* potential and rotational spectra of the CO-N<sub>2</sub> complex,  
797 *J. Chem. Phys.* 148 (2018) 044313.
- 798 [4] H. Cybulski, C. Henriksen, R. Dawes, X.-G. Wang, N. Bora, G. Avila,  
799 T. Carrington Jr., B. Fernández, *Ab initio* study of the CO-N<sub>2</sub> complex:  
800 a new highly accurate intermolecular potential energy surface and rovi-  
801 brational spectrum, *Phys. Chem. Chem. Phys.* 20 (2018) 12624–12636.
- 802 [5] N. D. Sze, Anthropogenic co emissions: Implications for the atmospheric  
803 co-oh-ch<sub>4</sub> cycle, *Science* 195 (1977) 673–675.
- 804 [6] S. C. Wofsy, Interactions of ch<sub>4</sub> and co in the earth’s atmosphere, *Annu.*  
805 *Rev. Earth Planet. Sci.* 4 (1976) 441–469.
- 806 [7] T. C. Owen, T. L. Roush, D. P. Cruikshank, J. L. Elliot, L. A.  
807 Young, C. De Bergh, B. Schmitt, T. R. Geballe, R. H. Brown, M. J.  
808 Bartholomew, Surface ices and the atmospheric composition of pluto,  
809 *Science* 261 (1993) 745–748.
- 810 [8] B. L. Lutz, C. De Bergh, T. Owen, Titan: Discovery of carbon monoxide  
811 in its atmosphere, *Science* 220 (1983) 1374–1375.
- 812 [9] D. P. Cruikshank, T. L. Roush, T. C. Owen, T. R. Geballe, C. De Bergh,  
813 B. Schmitt, R. H. Brown, M. J. Bartholomew, Ices on the surface of  
814 triton, *Science* 261 (1993) 742–745.
- 815 [10] N. Madhusudhan, S. Seager, A temperature and abundance retrieval  
816 method for exoplanet atmospheres, *Astrophys. J.* 707 (2009) 24.

- 817 [11] R. J. de Kok, M. Brogi, I. A. Snellen, J. Birkby, S. Albrecht, E. J.  
818 de Mooij, Detection of carbon monoxide in the high-resolution day-side  
819 spectrum of the exoplanet hd 189733b, *Astronomy & Astrophysics* 554  
820 (2013) A82.
- 821 [12] N. Madhusudhan, J. Harrington, K. B. Stevenson, S. Nymeyer, C. J.  
822 Campo, P. J. Wheatley, D. Deming, J. Blečić, R. A. Hardy, N. B. Lust,  
823 et al., A high c/o ratio and weak thermal inversion in the atmosphere  
824 of exoplanet wasp-12b, *Nature* 469 (2011) 64–67.
- 825 [13] C. He, S. M. Hörst, S. Riemer, J. A. Seabee, N. Pauley, V. Vuitton,  
826 Carbon monoxide affecting planetary atmospheric chemistry, *Astrophys.*  
827 *J. Lett.* 841 (2017) L31.
- 828 [14] S. M. Hörst, M. A. Tolbert, The effect of carbon monoxide on planetary  
829 haze formation, *Astrophys. J.* 781 (2014) 1–5.
- 830 [15] M. Woyde, W. Stricker, The application of cars for temperature mea-  
831 surements in high pressure combustion systems, *Appl. Phys. B* 50 (1990)  
832 519–525.
- 833 [16] R. Hall, Cars spectra of combustion gases, *Combust. Flame* 35 (1979)  
834 47–60.
- 835 [17] D. Klick, K. A. Marko, L. Rimai, Broadband single-pulse cars spectra  
836 in a fired internal combustion engine, *Appl. Opt.* 20 (1981) 1178–1181.
- 837 [18] J. H. Stufflebeam, A. C. Eckbreth, Cars diagnostics of solid propellant  
838 combustion at elevated pressure, *Combust. Sci. Technol.* 66 (1989) 163–  
839 179.
- 840 [19] V. Bergmann, W. Meier, D. Wolff, W. Stricker, Application of sponta-  
841 neous raman and rayleigh scattering and 2d lif for the characterization  
842 of a turbulent  $\text{ch}_4/\text{h}_2/\text{n}_2$  jet diffusion flame, *Appl. Phys. B* 66 (1998)  
843 489–502.
- 844 [20] T. Nakazawa, M. Tanaka, Measurements of intensities and self- and  
845 foreign-gas-broadened half-widths of spectral lines in the co fundamental  
846 band, *J. Quant. Spectrosc. Radiat. Transfer* 28 (1982) 409–416.

- 847 [21] T. Nakazawa, M. Tanaka, Intensities, half-widths and shapes of  
848 spectral lines in the fundamental band of CO at low temperatures,  
849 J. Quant. Spectrosc. Radiat. Transf. 28 (1982) 471–480.
- 850 [22] T. Drascher, T. F. Giesen, T. Y. Wang, N. Schmücker, R. Schieder,  
851 G. Winnewisser, P. Joubert, J. Bonamy, Temperature-dependent line  
852 shift broadening of co infrared transitions, J. Mol. Spectrosc 192 (1998)  
853 268–276.
- 854 [23] A. Predoi-Cross, C. Luo, P. M. Sinclair, J. R. Drummond, A. D. May,  
855 Line broadening and temperature exponent of the fundamental band in  
856 co-n<sub>2</sub> mixtures, J. Mol. Spectrosc 198 (1999) 291–303.
- 857 [24] A. Predoi-Cross, J. P. Bouanich, D. C. Benner, A. D. May, J. R. Drum-  
858 mond, Broadening, shifting, and line asymmetries in the 2←0 band of  
859 CO and CO–N<sub>2</sub>: Experimental results and theoretical calculations, J.  
860 Chem. Phys. 113 (2000) 158–168.
- 861 [25] A. Predoi-Cross, C. Hnatovsky, K. Strong, J. R. Drummond, D. C. Ben-  
862 ner, Temperature dependence of self- and n<sub>2</sub>-broadening and pressure-  
863 induced shifts in the  $j = 3 \leftarrow 0$  band of co, J. Mol. Struct. 695-696  
864 (2004) 269–286.
- 865 [26] B. J. Connor, H. Radford, Pressure broadening of the CO J = 1-0  
866 rotational transition by N<sub>2</sub>, O<sub>2</sub>, and air, J. Mol. Spectrosc. 119 (1986)  
867 229–231.
- 868 [27] J. Colmont, N. Monnanteuil, Self, nitrogen and oxygen broadening of the  
869 115-GHz line of carbon monoxide, J. Quant. Spectrosc. Radiat. Transf.  
870 35 (1986) 81–85.
- 871 [28] N. Nissen, J. Doose, A. Guarnieri, H. Mäder, V. N. Markov, G. Y.  
872 Golubyatnikov, I. I. Leonov, V. N. Shanin, A. F. Krupnov, Foreign gas  
873 broadening studies of the  $j' \leftarrow j = 1 \leftarrow 0$  rotational line of co by frequency  
874 and time domain techniques, Z. Naturforsch 54a (1999) 218–224.
- 875 [29] C. Puzzarini, L. Dore, G. Cazzoli, A comparison of lineshape models  
876 in the analysis of modulated and natural rotational line profiles: Appli-  
877 cation to the pressure broadening of ocs and co, J. Mol. Spectrosc 216  
878 (2002) 428–436.



- 879 [30] N. Semmoud-Monnanteuil, J. Colmont, Pressure broadening of millime-  
880 ter lines of carbon monoxide, *J. Mol. Spectrosc.* 126 (1987) 210–219.
- 881 [31] D. Priem, F. Rohart, J. M. Colmont, G. Wlodarczak, J. P. Bouanich,  
882 Lineshape study of the  $j = 3 \leftarrow 2$  rotational transition of co perturbed  
883 by  $n_2$  and  $o_2$ , *J. Mol. Struct.* 517-518 (2000) 435–454.
- 884 [32] V. N. Markov, G. Y. Golubiantnikov, V. A. Savin, D. A. Sergeev,  
885 A. Guarnieri, H. Mädler, Line broadening and shifting studies of the  
886  $j = 5 \leftarrow 4$  transition of carbon monoxide perturbed by co,  $n_2$ , and  $o_2$ ,  
887 *J. Mol. Spectrosc* (2002) 1–5.
- 888 [33] J.-M. Colmont, L. Nguyen, F. Rohart, G. Wlodarczak, Lineshape anal-  
889 ysis of the  $j = 3 - 2$  and  $j = 5 - 4$  rotational transitions of room  
890 temperature CO broadened by  $N_2$ ,  $O_2$ ,  $CO_2$  and noble gases, *J. Mol.*  
891 *Spectrosc* 246 (2007) 86–97.
- 892 [34] H. Józwiak, F. Thibault, H. Cybulski, P. Weisło, Ab initio investigation  
893 of the CO- $N_2$  quantum scattering: the collisional perturbation of the  
894 pure rotational R(0) line in CO, *J. Chem. Phys.* 154 (2021) 054314.
- 895 [35] M. Afzelius, C. Brackmann, F. Vestin, P.-E. Bengtsson, Pure rotational  
896 coherent anti-stokes raman spectroscopy in mixtures of CO and  $N_2$ ,  
897 *Appl. Opt.* 43 (2004) 6664–6672.
- 898 [36] P. S. Hsu, H. U. Stauffer, N. Jiang, J. R. Gord, S. Roy, Direct measure-  
899 ments of collisional raman line broadening in the s-branch transitions of  
900 co perturbed by co,  $n_2$ , and  $co_2$ , *Appl. Opt.* 58 (2019) C1–C6.
- 901 [37] A. Roblin, J. Bonamy, D. Robert, M. Lefebvre, M. Péalat, Rotational  
902 relaxation model for co- $n_2$ . prediction of cars profiles and comparison  
903 with experiment, *Journal de Physique II* 2 (1992) 285–294.
- 904 [38] M. Afzelius, P.-E. Bengtsson, J. Bonamy, Semiclassical calculations of  
905 collision line broadening in Raman spectra of  $N_2$  and CO mixtures, *J.*  
906 *Chem. Phys.* 120 (2004) 8616–8623.
- 907 [39] A. Owyong, E. D. Jones, Stimulated Raman spectroscopy using low-  
908 power cw lasers, *Opt. Lett.* 1 (1977) 152–154.

- 909 [40] R. S. McDowell, C. W. Patterson, A. Owyong, Quasi-cw inverse Raman  
910 spectroscopy of the  $\nu_1$  fundamental of  $^{13}\text{CH}_4$ , *J. Chem. Phys.* 72 (1980)  
911 1071–1076.
- 912 [41] P. Esherick, A. Owyong, High resolution stimulated Raman spec-  
913 troscopy, volume 9 of *Advances in IR and Raman Spectroscopy*, Heyden,  
914 1983.
- 915 [42] R. Z. Martínez, D. Bermejo, P. Wcisło, F. Thibault, Accurate wavenum-  
916 ber measurements for the  $S_0(0)$ ,  $S_0(1)$ , and  $S_0(2)$  pure rotational Raman  
917 lines of  $\text{D}_2$ , *J. Raman Spectrosc.* 50 (2019) 127–129.
- 918 [43] F. Thibault, R. Z. Martínez, D. Bermejo, L. Gómez, Collisional line  
919 widths of autoperperturbed  $\text{N}_2$ : Measurements and quantum calculations,  
920 *J. Quant. Spectrosc. Radiat. Transf.* 112 (2011) 2542–2551.
- 921 [44] R. Z. Martínez, D. Bermejo, Experimental determination of the rate of  
922 V–V collisional relaxation in  $^{14}\text{N}_2$  in its ground ( $X^1\Sigma_g^+$ ) electronic state  
923 between 77 and 300 K, *Phys. Chem. Chem. Phys.* 17 (2015) 12661–  
924 12672.
- 925 [45] F. Thibault, B. Corretja, A. Viel, D. Bermejo, R. Z. Martínez,  
926 B. Bussery-Honvault, Linewidths of  $\text{C}_2\text{H}_2$  perturbed by  $\text{H}_2$ : experiments  
927 and calculations from an ab initio potential, *Phys. Chem. Chem. Phys.*  
928 10 (2008) 5419–5428.
- 929 [46] G. Di Lonardo, L. Fusina, A. Baldan, R. Z. Martínez, D. Bermejo,  
930 High resolution infrared and Raman spectroscopy of  $\nu_2$  and associated  
931 combination and hot bands of  $^{13}\text{C}^{12}\text{CD}_2$ , *Mol. Phys.* 109 (2011) 2533–  
932 2542.
- 933 [47] F. Thibault, R. Z. Martínez, J. L. Domenech, D. Bermejo, J.-P.  
934 Bouanich, Raman and infrared linewidths of CO in Ar, *J. Chem. Phys.*  
935 117 (2002) 2523–2531.
- 936 [48] A. Lévy, N. Lacome, C. Chackerian, Collisional line mixing, in: K. N.  
937 Rao, A. Weber (Eds.), *Spectroscopy of the Earth’s Atmosphere and*  
938 *Interstellar Medium*, Academic Press, 1992, pp. 261–337.
- 939 [49] J.-M. Hartmann, C. Boulet, D. Robert, *Collisional Effects on Molecular*  
940 *Spectra*, Elsevier, Amsterdam, 2008.

- 941 [50] A. D. May, Molecular dynamics and a simplified master equation for  
942 spectral line shapes, *Phys. Rev. A* 59 (1999) 3495–3505.
- 943 [51] A. May, W.-K. Liu, F. McCourt, R. Ciuryło, J. S.-F. Stoker, D. Shapiro,  
944 R. Wehr, The impact theory of spectral line shapes: a paradigm shift,  
945 *Can. J. Phys.* 91 (2013) 879–895.
- 946 [52] G. J. Rosasco, W. Lempert, W. S. Hurst, A. Fein, Line interference  
947 effects in the vibrational Q-branch spectra of N<sub>2</sub> and CO, *Chem. Phys.*  
948 *Lett.* 97 (1983) 435–440.
- 949 [53] J. Boissoles, F. Thibault, J. L. Domenech, D. Bermejo, C. Boulet, J. M.  
950 Hartmann, Temperature dependence of line mixing effects in the stim-  
951 ulated raman Q-branch of CO in He: A further test of close coupling  
952 calculations, *J. Chem. Phys.* 115 (2001) 7420–7428.
- 953 [54] P. W. Rosenkranz, Shape of the 5 mm Oxygen Band in the Atmosphere,  
954 *IEEE Transactions on Antennas and Propagation AP-23* (1975) 498–  
955 506.
- 956 [55] R. Ciuryło, J. Szudy, Line-mixing and collision-time asymmetry of spec-  
957 tral line shapes, *Phys. Rev. A* 63 (2001) 042714.
- 958 [56] N. Anselm, K. Yamada, R. Schieder, G. Winnewisser, Measurements of  
959 foreign gas pressure shift and broadening effects in the (1-0) band of CO  
960 with N<sub>2</sub> and Ar, *J. Mol. Spectrosc.* 161 (1993) 284–296.
- 961 [57] A. Hamdouni, A. Barbe, J.-J. Plateaux, V. Langlois, V. Dana, J.-Y.  
962 Mandin, M. Badaoui, Measurements of N<sub>2</sub>-induced shifts and broad-  
963 ening coefficients of lines in CO fundamental from Fourier transform  
964 spectra, *J. Quant. Spectrosc. Radiat. Transf.* 50 (1993) 247–255.
- 965 [58] J. Mandin, V. Dana, M. Badaoui, A. Barbe, A. Hamdouni, J. Plateaux,  
966 Measurements of pressure-broadening and pressure-shifting coefficients  
967 from FT spectra, *J. Mol. Spectrosc.* 164 (1994) 328–337.
- 968 [59] P. Sinclair, P. Duggan, R. Berman, A. May, J. Drummond, Line broad-  
969 ening, shifting, and mixing in the fundamental band of CO perturbed  
970 by N<sub>2</sub> at 301 K, *J. Mol. Spectrosc.* 181 (1997) 41–47.

- 971 [60] C. Luo, R. Berman, A. Predoi-Cross, J. Drummond, A. May, Lineshifts  
972 in the fundamental band of CO: Confirmation of experimental results for  
973  $\text{n}_2$  and comparison with theory, *J. Mol. Spectrosc* 196 (1999) 290–295.
- 974 [61] D. A. Long, *The Raman Effect*, John Wiley & Sons Ltd., Chichester,  
975 West Sussex, England, 2002.
- 976 [62] L. Gomez, R. Z. Martínez, D. Bermejo, F. Thibault, P. Joubert,  
977 B. Busseron-Honvault, J. Bonamy, Q-branch linewidths of  $\text{N}_2$  perturbed  
978 by  $\text{H}_2$ : Experiments and quantum calculations from an ab initio poten-  
979 tial, *J. Chem. Phys.* 126 (2007) 204302.
- 980 [63] F. Thibault, L. Gomez, S. V. Ivanov, O. G. Buzykin, C. Boulet, Com-  
981 parison of quantum, semi-classical and classical methods in the calcula-  
982 tion of nitrogen self-broadened linewidths, *J. Quant. Spectrosc. Radiat.*  
983 *Transf* 113 (2012) 1887–1897.
- 984 [64] F. Thibault, R. Z. Martínez, D. Bermejo, S. V. Ivanov, O. G. Buzykin,  
985 Q. Ma, An experimental and theoretical study of nitrogen-broadened  
986 acetylene lines, *J. Quant. Spectrosc. Radiat. Transf* 142 (2014) 17–24.
- 987 [65] S. Green, Rotational excitation in  $\text{H}_2$ - $\text{H}_2$  collisions: Close-coupling cal-  
988 culations, *J. Chem. Phys.* 62 (1975) 2271–2277.
- 989 [66] S. Green, Raman linewidths and rotationally inelastic collision rates in  
990 nitrogen, *J. Chem. Phys.* 98 (1993) 257–268.
- 991 [67] J. M. Hutson, S. Green, MOLSCAT version 14, Collaborative Compu-  
992 tational Project 6 of the UK Science and Engineering Research Council,  
993 Daresbury Laboratory, UK (1995).
- 994 [68] J. M. Hutson, C. R. L. Sueur, molscat: A program for non-reactive quan-  
995 tum scattering calculations on atomic and molecular collisions, *Comput.*  
996 *Phys. Commun.* 241 (2019) 9–18.
- 997 [69] S. Hess, Kinetic theory of spectral line shapes. The transition between  
998 Doppler broadening and collisional broadening, *Physica* 61 (1972) 80–  
999 94.
- 1000 [70] G. C. Corey, F. R. McCourt, Dicke narrowing and collisional broadening  
1001 of spectral lines in dilute molecular gases, *J. Chem. Phys.* 81 (1984)  
1002 2318–2329.

- 1003 [71] L. Monchick, L. W. Hunter, Diatomic-diatomic molecular collision in-  
1004 tegrals for pressure broadening and Dicke narrowing: A generalization  
1005 of Hess's theory, *J. Chem. Phys.* 85 (1986) 713–718.
- 1006 [72] L. Demeio, S. Green, L. Monchick, Effects of velocity changing collisions  
1007 on line shapes of HF in Ar, *J. Chem. Phys.* 102 (1995) 9160–9166.
- 1008 [73] R. Z. Martínez, D. Bermejo, F. Thibault, P. Wcisło, Testing the ab  
1009 initio quantum-scattering calculations for the D<sub>2</sub>–He benchmark system  
1010 with stimulated Raman spectroscopy, *J. Raman Spectrosc.* 49 (2018)  
1011 1339–1349.
- 1012 [74] F. Thibault, R. Z. Martínez, D. Bermejo, P. Wcisło, Line-shape param-  
1013 eters for the first rotational lines of HD in He, *Mol. Astrophys.* 19 (2020)  
1014 100063.
- 1015 [75] A. P. Yutsis, I. B. Levinson, V. V. Vanagas, Jerusalem: Israel Program  
1016 for Scientific Translations, 1962.
- 1017 [76] J. Schaefer, L. Monchick, Line shape cross sections of HD immersed in  
1018 He and H<sub>2</sub> gas. I. Pressure broadening cross sections, *J. Chem. Phys.*  
1019 87 (1987) 171–181.
- 1020 [77] J. Schaefer, L. Monchick, Line broadening of HD immersed in He and  
1021 H<sub>2</sub> gas, *Astron. Astrophys.* 265 (1992) 859–868.
- 1022 [78] U. Fano, Pressure broadening as a prototype of relaxation, *Phys. Rev.*  
1023 131 (1963) 259–268.
- 1024 [79] A. Ben-Reuven, Impact broadening of microwave spectra, *Phys. Rev.*  
1025 145 (1966) 7–22.
- 1026 [80] R. Blackmore, S. Green, L. Monchick, Polarized D<sub>2</sub> Stokes–Raman  
1027 Q branch broadened by He: A numerical calculation, *The Journal of*  
1028 *Chemical Physics* 88 (1988) 4113–4119.
- 1029 [81] F. Thibault, H. Józwiak, Code for pressure broadening, shift and com-  
1030 plex Dicke cross sections for 2 diatomics, *Mendeley Data*, V2, doi:  
1031 10.17632/tdvgvwr2t7.2, 2021.
- 1032 [82] M. Baranger, General impact theory of pressure broadening, *Phys. Rev.*  
1033 112 (1958) 855–865.

- 1034 [83] A. E. DePristo, H. Rabitz, The effect of elastic and reorientation col-  
1035 lisions on vibration-rotation lineshapes: A semi-empirical approach, *J.*  
1036 *Quant. Spectrosc. Radiat. Transf* 22 (1979) 65–79.
- 1037 [84] R. Blackmore, A modified Boltzmann kinetic equation for line shape  
1038 functions, *The Journal of Chemical Physics* 87 (1987) 791–800.
- 1039 [85] F. Thibault, B. Calil, J. Boissoles, J. M. Launay, Experimental and  
1040 theoretical CO<sub>2</sub>–He pressure broadening cross sections, *Phys. Chem.*  
1041 *Chem. Phys.* 2 (2000) 5404–5410.
- 1042 [86] F. Thibault, B. Calil, J. Buldyreva, M. Chrysos, J.-M. Hartmann, J.-P.  
1043 Bouanich, Experimental and theoretical CO<sub>2</sub>–Ar pressure-broadening  
1044 cross sections and their temperature dependence, *Phys. Chem. Chem.*  
1045 *Phys.* 3 (2001) 3924–3933.
- 1046 [87] F. Thibault, E. Fuller, K. Grabow, J. Hardwick, C. Marcus, D. Marston,  
1047 L. Robertson, E. Senning, M. Stoffel, R. Wisner, Experimental line broad-  
1048 ening and line shift coefficients of the acetylene  $\nu_1 + \nu_3$  band pressurized  
1049 by hydrogen and deuterium and comparison with calculations, *J. Mol.*  
1050 *Spectrosc* 256 (2009) 17–27.
- 1051 [88] F. Thibault, Pressure broadening and shift code for 2 diatomics - coupled  
1052 states approximation, *Mendeley Data*, V2,doi: 10.17632/ykxz36nwry.2,  
1053 2020.
- 1054 [89] E. W. Smith, Absorption and dispersion in the O<sub>2</sub> microwave spectrum  
1055 at atmospheric pressures, *J. Chem. Phys.* 74 (1981) 6658–6673.
- 1056 [90] F. Thibault, J. Boissoles, R. Le Doucen, R. Farrenq, M. Morillon-  
1057 Chapey, C. Boulet, Line-by-line measurements of interference param-  
1058 eters for the 0–1 and 0–2 bands of CO in He, and comparison with  
1059 coupled-states calculations, *J. Chem. Phys.* 97 (1992) 4623–4632.
- 1060 [91] A. E. DePristo, H. Rabitz, On the use of various scaling theories in the  
1061 deconvolution of rotational relaxation data: Application to pressure-  
1062 broadened linewidth measurements, *J. Chem. Phys.* 69 (1978) 902–911.
- 1063 [92] F. Thibault, K. Patkowski, P. Zuchowski, H. Jóźwiak, P. Wcisło,  
1064 R. Ciuryło, Rovibrational line-shape parameters for H<sub>2</sub> in He and new

- 1065 H<sub>2</sub>-He potential energy surface, *J. Quant. Spectrosc. Radiat. Transfer*  
1066 202 (2017) 308.
- 1067 [93] H. Jóźwiak, F. Thibault, N. Stolarczyk, P. Wcisło, Ab initio line-shape  
1068 calculations for the S and O branches of H<sub>2</sub> perturbed by He, *J. Quant.*  
1069 *Spectrosc. Radiat. Transf* 219 (2018) 313–322.
- 1070 [94] J. O. Hirschfelder, C. F. Curtiss, R. B. Bird, *Molecular Theory of Gases*  
1071 *and Liquids*, Wiley, 4th edition, 1967.
- 1072 [95] G. Kowzan, H. Cybulski, P. Wcisło, M. Słowiński, A. Viel, P. Masłowski,  
1073 F. Thibault, Subpercent agreement between ab initio and experimental  
1074 collision-induced line shapes of carbon monoxide perturbed by argon,  
1075 *Phys. Rev. A* 102 (2020) 012821.
- 1076 [96] A. Mantz, F. Thibault, J. Cacheiro, B. Fernandez, T. Pedersen, H. Koch,  
1077 A. Valentin, C. Claveau, A. Henry, D. Hurtmans, Argon broadening of  
1078 the <sup>13</sup>CO R(0) and R(7) transitions in the fundamental band at tem-  
1079 peratures between 80 and 297 K: comparison between experiment and  
1080 theory, *J. Mol. Spectrosc* 222 (2003) 131–141.
- 1081 [97] W. Deng, D. Mondelain, F. Thibault, C. Camy-Peyret, A. W. Mantz,  
1082 Experimental He-pressure broadening for the R(10) and P(2) lines in the  
1083  $\nu_3$  band of <sup>13</sup>CO<sub>2</sub>, and experimental pressure shifts for R(10) measured  
1084 at several temperatures between 300K and 100K, *J. Mol. Spectrosc* 256  
1085 (2009) 102–108.